Biospeckle-based Study of the Line Profile of Light Scattered in Strawberries

Master Thesis
by
Anders Bergkvist

Lund Reports on Atomic Physics, LRAP-220
Lund 1997

This thesis was carried out at
Centro de Investigaciones Opticas (CIOp) in La Plata, Argentina,
and submitted to the
Faculty of Technology at Lund University
in partial fulfilment of the requirements for the degree of
Master of Science

Abstract

The line profiles of light scattered in strawberries were measured with a biospeckle approach. This method allows studies of extremely small shifts (0.1 Hz) in matter consisting of randomly moving particles. The method is independent of the number and types of particles in the object. 512 timehistories of different areas in the speckle pattern were simultaneously recorded. The timehistories were autocorrelated and Fourier transformed to obtain the frequency spectra of the scattered light. This line profile was compared with a Voight profile to determine the ratio of Lorentzian to Gaussian line shape in it. It was found that Lorentzian line profile originates from diffusive movements in the object and the Gaussian from turbulent movements as well as from speed of particles in the object. The changes in diffusive activity correlates with changes in the cell wall structure, and the changes in Gaussian line width correlates with the flow of particles into the vacoules of the cells.

Table of contents

1. Introduction

1.1 Background

Strawberries belong to a group called soft fruits. The characteristics of that group is simply that they lack firm texture. They are a fresh product with a very short post harvest shelf life. The commercial handling is therefore kept to a minimum to reduce damage. For the same reason refrigeration during transport and storage is a common move to slow down the process. As a natural consequence the majority of the soft fruits are processed to jams, juices, and canned and frozen fruit. Since the usefulness of strawberries to a great extent depends on the textural changes, it is an important task to learn how to measure it. A fast and elegant way of doing this would be with a method using light.

The idea arose in the Rio Negro area in Argentina where apple farmers export large amounts of fruit to other continents every year. The apples mature on the ship during the trip to arrive fresh to the customer. If the fruit matures too early it turns bad and if it matures too late it will cause costs in storage. It is therefore crucial for the farmers to know the optimal time for harvesting their fruit. This would be possible to do if they had an instrument that determines the maturity of fruit, for instance by using optics.

Atomic physics and optics offer people elegant ways of discovering, measuring and treating things the naked eye can not see. Whether it is light from interstellar space or induced fluorescence from a banana, it always involves electromagnetic radiation as a bearer of information. However, when investigating biological samples, great problems are encountered because of the complexity of the objects. The matter consists of incredibly many types of particles, which consist of many kinds of molecules, atoms and bonds. On top of this, the matter is not homogenous and changes its properties with time. All together, this limits the possibilities for isolating single line profiles in the measurements. In this thesis the activity in objects is measured with a technique based on time varying speckles, which overcomes many of these problems.

Many different methods have been used to measure the activity but most of them have limits which makes it difficult to obtain an accurate description of the object. A study with microscope is a destructive process since the object needs to be sectioned. Laser

Doppler velocimetry measures the flow of particles in a certain direction and consequently does not detect random movement. Laser spectroscopy is a remarkable instrument for extracting information about a medium, but it is far too rough to measure the shifts caused by changes in the activity. The time varying speckle approach however, can be used to do experiments independent of the number and types of particles in the object. This technique measures quality rather than quantity of light and manages shifts within a few hertz.

The time varying speckle phenomenon has already been used to study a variety of objects that move in random ways. For example during the drying process of paint, the moving particles in it have been observed. The particles in the wet paint keep moving until the paint is completely dry [1]. The blood flow in superficial layers of skin has successfully been studied in [2], the activity of micro-organisms in a solution in [3] and the decadence of fresh fruit in [4]. What they all have in common is that only the Doppler velocity of the particles in the matter is measured. Since the light scattered from the object contains a lot more information about the processes in the matter, it ought to be possible to extract it. This would lead to a possibility to solve the two problems concerning apples and strawberries.

1.2 Objectives

The objective of this thesis is to extract information from biospeckles about how changes in cells influence light that is scattered inside the cells. The study is focused on how the line profile of the scattered light changes with the activity in the fruits. Furthermore it is analysed if the scattered light can be described with the Voight profile. Finally, as far as possible, the line profile is used to determine the maturity of fruits.

1.3 Limitations

The statistical properties and mathematics for biospeckles have not yet been established because of the complexity of the movements of living objects. I have therefore an experimental approach to this study. Since the biological tissue is such a complex medium, not only consisting of a large amount of different matters but is also non-homogeneous, it is necessary to do approximations to get an applicable model to work with. The matter is therefore regarded as homogeneous with a seedless surface and the internal activity independent of the depth in the tissue.

Because of the limited extent of this study it is not supplemented with simulations about the optical properties of fruit tissue. However, some of them have previously been measured which gives an idea about the properties in the matters used in this work [4,5,6]. For the same reason the biospeckle experiments are not combined with other techniques (like for instance spectroscopy) to get a more complete representation of the objects.

2. Theoretical Aspects

2.1. Light interaction with biological tissue

2.1.1 Light-matter interaction

Light interacts with matter in various ways, figure 1. The different processes that occur depend on the wavelength of the light as well as the structure of the medium. Light can be reflected, scattered or absorbed when it interacts with the matter. Photons with very high energy, like gamma and x-rays, may even ionise atoms or break bonds in the molecules, but this will not be the case in this work since visible light is being used through all the experiments.

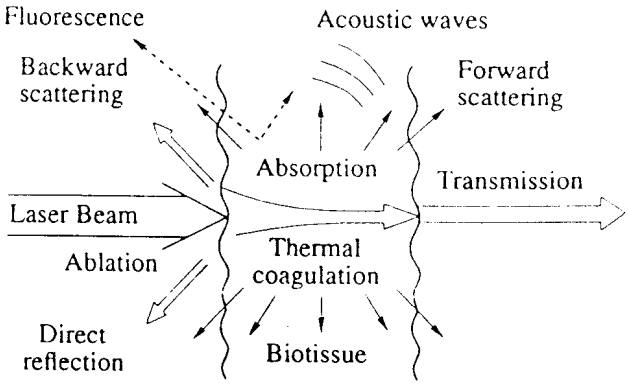

Figure 1. Various interactions between light and matter [7].

The reflection of the light, when it enters a border between different refractive indexes, obeys the laws of Snell and Fresnel. It depends therefore on the refractive indexes as well as the angle of the incoming and the reflected rays:

$$n_1 \cdot \sin\varphi_1 = n_2 \cdot \sin\varphi_2 \qquad \text{(Snell)} \qquad (1)$$

$$R = \frac{1}{2}\left[\frac{\sin^2(\varphi_1 - \varphi_2)}{\sin^2(\varphi_1 + \varphi_2)} + \frac{\tan^2(\varphi_1 - \varphi_2)}{\tan^2(\varphi_1 + \varphi_2)}\right] \qquad \text{(Fresnel)} \qquad (2)$$

n_1, n_2 are the refractive indexes in the two materials and φ_1, φ_2 the angles of the light perpendicular to the boundary.

The scattering can be either elastic or inelastic. Elastic means that the scattered photons neither loose nor gain energy in the process. The types of elastic scattering are Rayleigh and Mie. In Rayleigh scattering, the electromagnetic field of the incoming light induces a polarisation of the molecule, which ”re-radiates” the light with retained wavelength and without delay. This appears when the particles in the substance are about the same size as or smaller than the wavelength of the light, figure 2. The cross section for this process is about 10^{-26} cm^{-2} and proportional to λ^{-4} [8], which means that it increases as the wavelength decreases. This involves, for instance, that the blue

light from the sun is scattered on the molecules in the air more than the red light, and therefore makes the sky look blue.

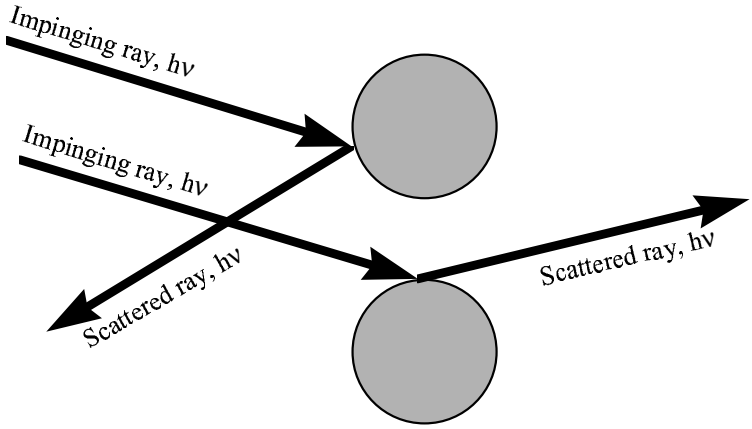

Figure 2. Rayleigh scattering on particles.

If the particles on the other hand are bigger than the wavelength, there will be Mie scattering. In this case a ray simply penetrates the wall of the particle and reflects one or several times against the inside of the wall before it leaves the particle, figure 3. Examples of this are the bad visibility in fog and the rainbow in the clouds. In the latter example, the sunlight scatters in the water drops in the clouds. As the sunlight consists of a wide spectra, the drops in the clouds will operate as small prisms which scatter the different wavelengths in different angles to the sun, and there will be a rainbow. The cross section for Mie scattering depends very much on the sizes and refractive indexes of the particles and the surrounding media. It varies therefore between about 10^{-26} and 10^{-8} cm^{-2} [8]. The probability of the effect is proportional to λ^{-2} and is hence not as wavelength dependent as Rayleigh scattering.

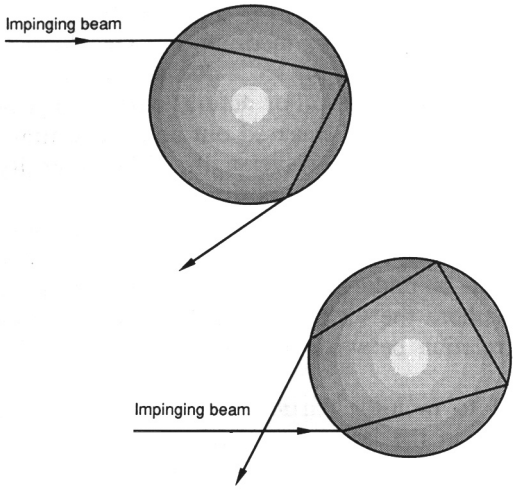

Figure 3. Mie scattering in particle.

The strongest inelastic effects in scattered light are Raman and Brillouin. Raman is a special case of Rayleigh scattering. The difference appears when the molecule re-radiates the light. The excited electrons fall back to another energy level than where

they were before the polarisation, figure 4. This gives wavelengths shifted certain energies, up or down, from the wavelength of the incoming light, specific for each bond in the medium. Hydrogen has the largest shift and changes the energy 4155 cm^{-1}, but the most common shifts are 100-1000 cm^{-1} [9]. The cross section for Raman scattering is about 10^{-29} cm^{-2}.

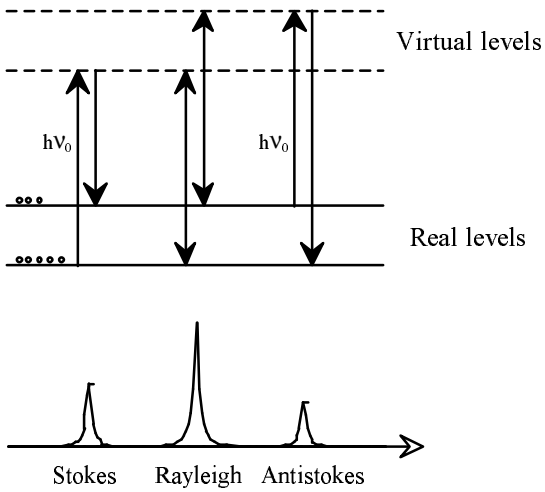

Figure 4. Raman shifts of the scattered light [8].

Brillouin scattering appears when a crystal is deformed by a long acoustic phonon. The refractive index of the crystal changes due to the tension that is induced by the vibration. Consequently, if a phonon is present it will affect the shifts and directions of all the photons it encounters. The size of the changes, depends on the resonance frequencies of the setup and hence the characteristics and size of the object, the laboratory, the equipment and the phonon.

The absorption process is a very complex part of the interaction. The different atoms and molecules in the matter have a wide range of possible energy levels which can be excited. After a certain time delay, also depending on the type of atoms or molecules, they loose energy by either producing heat, contributing to some photochemical reaction or re-radiate photons in any direction, called fluorescence. These photons may have the same wavelengths as the incoming rays but also other, depending on the probability for the occupation of the different energy levels. All this information is specific for each medium and is therefore a good source when working with spectroscopy to extract information concerning the characteristics of the substance. On the other hand, since this study is depending on the correlation of the scattering in different media, the re-radiation may instead be a source of noise. The probabilities for absorption and fluorescence are both normally about 10^{-16} cm^{-2}. However, in liquids and solids at atmospheric pressure the molecules will be close enough to bounce in to each other and stimulate the segregation of heat. This is called quenching and reduces the probability of fluorescence to about 10^{-20} cm^{-2} [8].

2.1.2. Composition and structure of biological tissue

All biological tissue consist of cells. Figure 5 shows a typical vegetable cell, its basic elements and their sizes. The diameter of the cell is about 0.1 mm. The cell wall is a 30 nm thick layer of polysaccharides and proteins that will stretch as the cell grows and eventually deteriorate and break as the cell dies. In the cell there are several nuclei with the size of about 0.5 μm which includes the DNA. The mitochondria have about the same size as the nuclei and control the respiration of the cell, as it provokes the oxidation of nutrients. There are also larger parts, chloroplasts, which are the engines of the cells. They are a few μm in diameter, contain chlorophyll and are responsible for the production of energy. The ligament that glues the particles together consists of endoplasmic reticulum which produces and transports proteins to the membranes. The biggest part of the cell is the vacuole, which is a reservoir of water, sugars, pigments, oxygen and carbon dioxide. It is the part that expands the most and makes the cell grow.

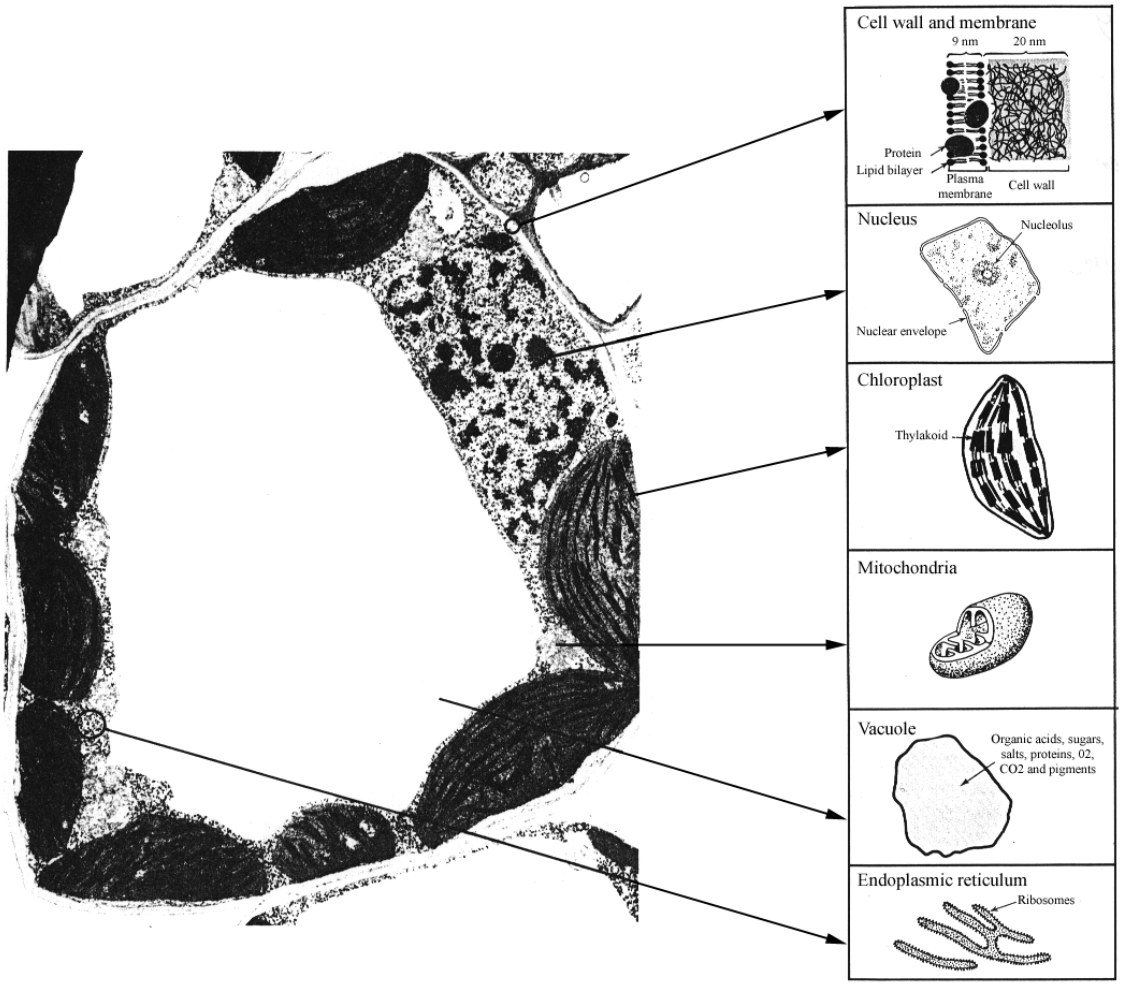

Figure 5. Vegetable cell [10].

The cells stick to each other like bricks in a wall, even though there is interspace between some of them. This space may be filled with air or loose subparts of cells. The tissue has a 50 μm thick layer of surface cells that are called epidermal cells. The

surface is normally covered with wax, small fluff called trichomes and pigments to moderate the wavelengths that penetrate it. Leaves which have been extensively studied have more layers. Their next layer is called palisade and is about 1 mm thick. Underneath is the spongy layer which has about the same thickness [11].

The distribution of chloroplasts is not homogenous right the way through the tissue. It highly depends on the type of vegetable and where it grows. When it grows in the shade and is reached by diffuse light, it needs another distribution than if it receives direct collimated light. It also has a movement of the chloroplasts, called cyclosis, to adjust the absorption of light. There is even a movement of whole cells to use the light as effectively as possible. As the light penetrates the tissue, the intensity decreases with the depth and the cells turn towards the highest gradient of the light. In other words, the biological tissue is not a "vegetable", it is actively working to influence light propagation and absorption to its own advantage.

2.1.3. Optical properties of biological tissue

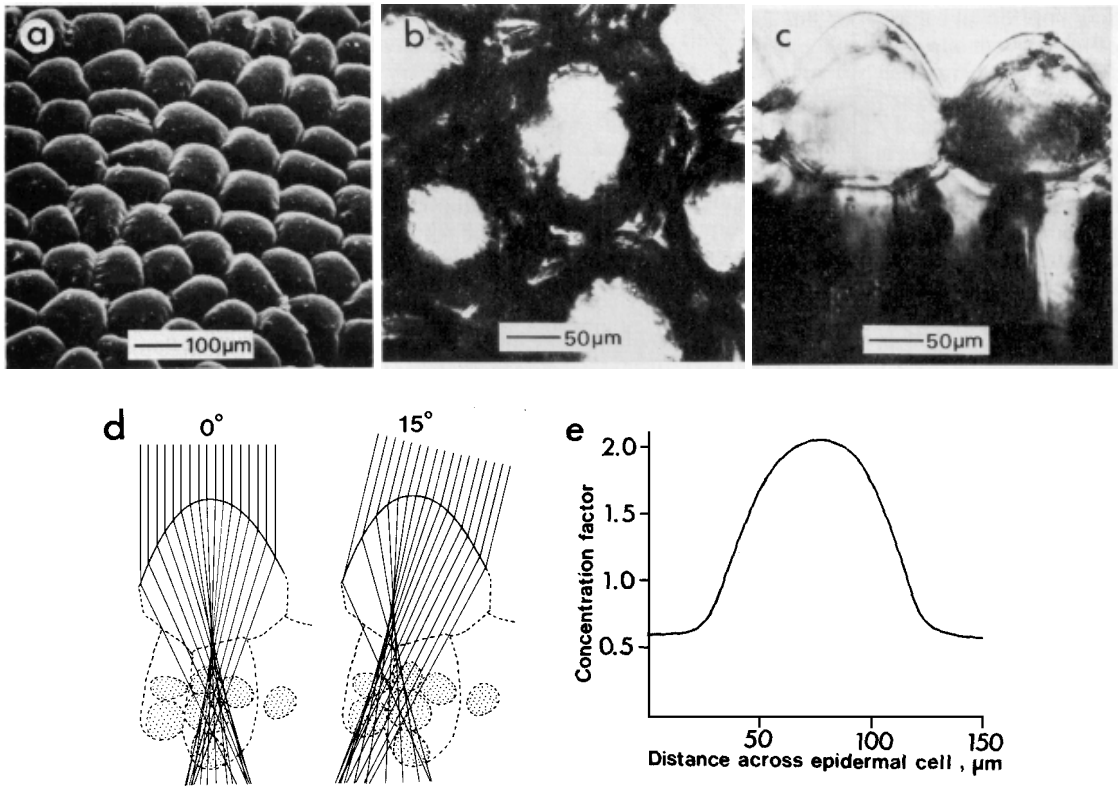

Figure 6. (a) Surface of vegetable showing cells. **(b,d)** Cells (seen from above) focusing light towards their centres. **(c)** Cells (seen from the side) focusing light. **(e)** Intensity concentration in cells. [12].

Any transparent matter with a curved surface and a refractive index higher than air, can focus light. Tissue has absorption centres, consisting of so called chromophores. It is in these centres that the tissue can optimise its use of light, consequently cells concentrate the incoming light to these areas. This is particularly important for leaves because they are thin and need to create a lot of energy to support the plant. Figure 6 shows epidermal cells of a tropical plant, living in the shade, with very strong focusing. Even though it is hard to imagine a lens effect in a matter with multiple

scattered light, calculations of radiation within maize mesocotyls, the first leaves of the sprout, indicate that focusing further into the tissue could exist [5]. Obviously the electromagnetic field in biological tissue is very heterogeneous and the concentrations of light vary a lot.

Let us now reason microscopically about the scattering with the above mentioned types of interactions with matter; reflection, scattering and absorption. As the tissue has a higher refractive index than air, there will be a reflection on the surface. The light that penetrates however, may therefore also be trapped inside. If polarised light is used, it will loose its polarisation at a high exponential rate as it penetrates the tissue. Therefore approximately all the light that is reflected back with kept polarisation comes from the reflection in the surface [4,5]. During a study, when illuminating biological tissue with polarised light, researchers found that the polarisation in the specular direction of observation was 0.98 due to the reflection in the surface but only 0.17 in a 0°/30° setup (similar to the one that is used in this study).

The refractive indexes are different inside and outside the cells as well as in all the cell parts and in the cell wall. The indexes of different vegetable cell walls have been investigated with results between 1.333-1.472 and with an average of 1.425 [6]. This means that the back scattered light from biological tissue not only is multiple scattered, but is also multiple reflected on different surfaces.

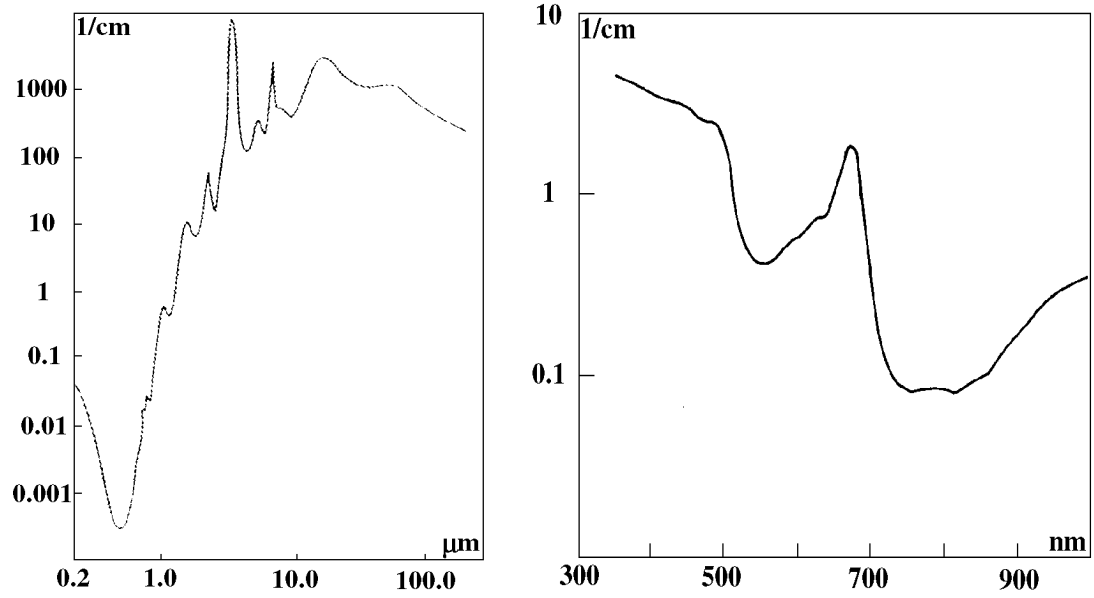

Figure 7. Light absorption in water (left) and chlorophyll (right).

Biological tissue is a highly scattering media. The sizes of the cells, the vacuoles and spaces between cells are a bit larger than the wavelength of a HeNe-laser. Thus they are probably participating in Mie scattering, which consequently is very strong with a cross section comparable with the absorption, 10^{-16} cm^{-2}. All the other parts as well as all the molecules are participating in the Rayleigh scattering. The cross section for Rayleigh scattering, 10^{-26} cm^{-2}, is however small compared to that for Mie scattering. This also leads to that the Raman effect is very small as the cross section is about 10^{-29} cm^{-2}. There is also Brillouin-scattering in biological tissue even though it is not as

strong as in a crystal. These effects will cause direct or indirect shifts and broadenings in the scattered light. This will be further discussed in chapter 2.4.

The absorption is wavelength dependent and varies a lot. Due to that the main absorbers are water and chlorophyll, the absorption spectrum mainly depends on them. In figure 7, the absorption spectra for water and chlorophyll are illustrated. Note that they have different scales of wavelength. We can see that water absorbs a lot in the infrared region, yet it has a window at around 0.6 μm. A HeNe-laser is therefore a good source to use if you do not want to get your signal absorbed by water. The chlorophyll naturally absorbs of course a lot in the visible range, since that is its main purpose. One of the chlorophyll's absorption peaks coincides with the wavelength of the laser, 633 nm. This greatly facilitates measurements of the amount of chlorophyll in an object. When measuring speckles, a strong absorption does not cause important problems. However, when measuring an object where the quantity of chlorophyll changes a lot, changes in the speckle size may occur with time as less absorption involves deeper penetration of the light. By using a diaphragm, it is possible to get rid of this problem since this method keeps the speckle size constant.

Most of the absorbed energy will turn into heat but the change of temperature will probably not be important even though there is a strong absorption. Let us for example calculate how much the energy in the object increases due to the setup I am using in this study. I illuminate a disc with 2 mm in diameter and a thickness of about 3 mm, which is approximately $0.001^2 \cdot \pi \cdot 0.003 \cdot 1000$ kg = 10 mg water, with a 10 mW HeNe laser during about 40 s. Due to an imperfect polariser only 50 % of the laserbeam reaches the object. The object will hence increase $\Delta T = \frac{\Delta W}{m \cdot C_v} \cdot 0.5$ K = $\frac{10 \cdot 10^{-3} \cdot 40}{10 \cdot 10^{-6} \cdot 4.18 \cdot 10^3} \cdot 0.5$ K = 5 K in temperature. However, this approximation assumes that no light is neither scattered nor reflected from the object. Furthermore, there will be convection with the rest of the object as well as the air and the object will radiate energy from its surface. All together the increased temperature will be limited to only a few Kelvin.

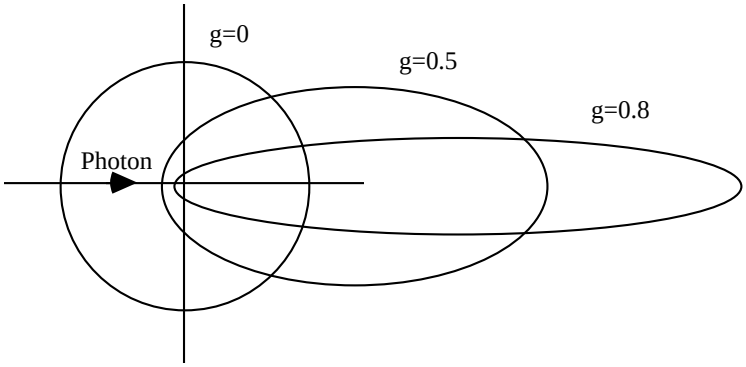

Figure 8. The probability for a photon to be scattered in certain directions for different values of g.

The most common way of describing the properties of a medium is with the absorption coefficient, μ_a, and scattering coefficient, μ_s. To get the total coefficient, the two are coupled to define the linear transport coefficient $\mu_{tr} = \mu_s' + \mu_a$. μ_s' is the reduced scattering coefficient $\mu_s' = (1-g)\mu_s$ which depends on the anisotropy factor g. g is the mean cosine of the scattering angle and can obtain values between -1 and 1. g=1 is pure forward scattering and g=0 is uniform scattering, figure 8. Human tissue, for example, has a typical value of the factor g=0.7-0.95 [13]. To get an idea of the coefficients in a strawberry I mention some experimental values for a cotyledon of cucurbita pepo, which is a leaf; μ_a=0.8 mm^{-1} and μ_s=2.2 mm^{-1}.

These coefficients will however not be used in this work. The scattering is of far greater importance than the absorption and it is instead necessary to differ the types of scatterings included in μ_s from each other.

2.2. Speckles

2.2.1. Laser speckles

When a laser beam hits an object or is transmitted through a diffuse space, the place of the impact will be a spot with a granular appearance. When you move sideways, the pattern as a whole will also move sideways, but if you move closer or further away from the object, the pattern will change its appearance. The phenomenon is called speckles and has its origin in the roughness of a surface combined with the coherent laser light, figure 9. The photons from the spot will interfere constructively or destructively with each other in every observation plane that is reached by the light, and there form a random pattern of grains, figure 10.

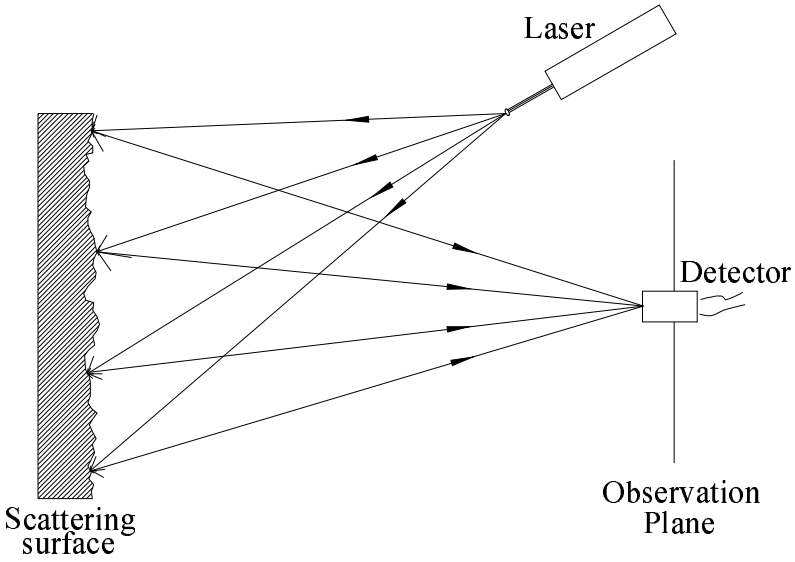

Figure 9. Speckles created at a rough surface.

For example, if you look at the spot, your retina will be one of these planes, as in the example above. As many waves from different parts of the spot interact, they all have different phases, creating an intensity consisting of their complex sum, figure 11 and equation 5. The intensity function, which is a result from a ray-tracing function, is an exponential function [14];

$$P_I(I) = \frac{I}{< I >} e^{\left(\frac{I}{<I>}\right)} \tag{3}$$

where $P_I(I)$ is the probability of a certain intensity I. The intensity with highest probability is 0, the mean intensity $< I >$, and for higher values it falls off rather quickly. This means that the variations of the intensities are not very big and therefore sensitive to noise.

The size of each speckle follow the law of Airy:

$$d = 2 \cdot 1.22\left(\frac{\lambda \cdot z}{D}\right) \tag{4}$$

where d = diameter of speckles, z = distance of observation and D = diameter of circular area observed.

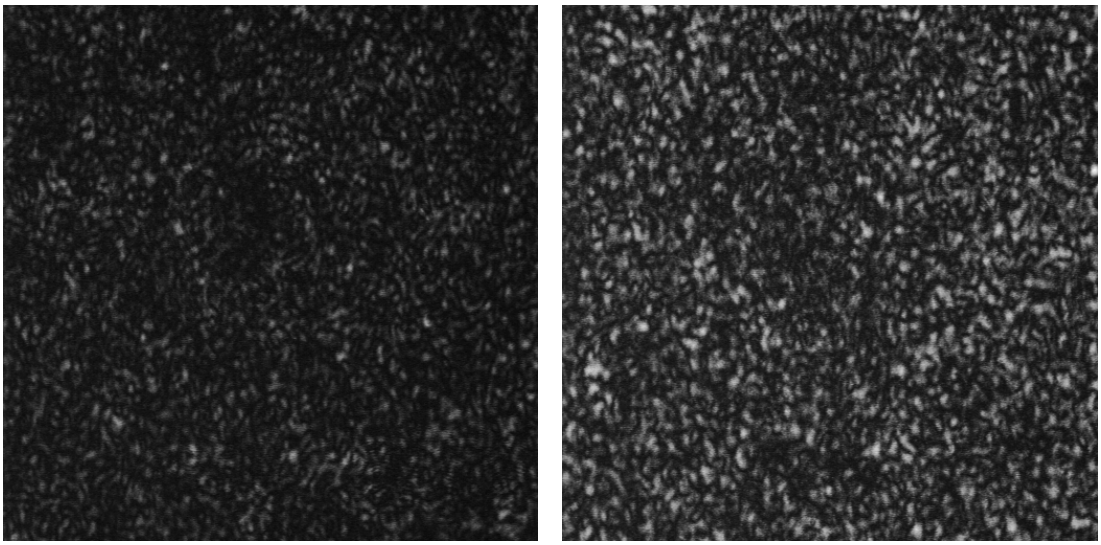

Figure 10. Speckle pattern from a strawberry. Analyser and polariser perpendicular (left) and parallel (right).

2.2.2. Biospeckles

When speckles are created from light scattered by moving particles, the speckles are modulated by the state of motion of the scatterers. This makes the speckle pattern time varying and thus the speckles are called temporal. It actually gives the speckles a boiling appearance and they are therefore sometimes referred to as boiling speckles. When the speckles originate from biological specimen the speckles are called biospeckles. Biospeckles stern from a very complex phenomenon. When the light penetrates the object it is multiple scattered in all possible directions before leaving the object. Consequently it is not possible to recognise and study each particle that scatters the light. In each point in the speckle image, the light from many scatterers are superposed and therefore complexly added. The resulting intensity is

$$A(P,t) = \sum_{j=1}^{N} \left|A_j(P,t)\right| \exp\left[i\phi_j(P,t)\right] \tag{5}$$

where A is the phase amplitude, P the observation point and N the number of scatterers that contribute to A in P. Compare with the complex addition in figure 11. This is identical with the random walk problem in two dimensions [15]. The frequency of the speckle fluctuations are hence directly related to the rate of change in the random walk and therefore the velocity of each scatterer. The effect can be compared with the

Doppler method where a very narrow laser beam illuminates a vessel and the velocity ($\overline{v}$) of the fluid in the vessel is given from the frequency of the fluctuating scattered light:

$$f_D = \frac{1}{2\pi}(\overline{K}_s - \overline{K}_i)\cdot\overline{v} \qquad (6)$$

where $\overline{K}_s$ and $\overline{K}_i$ are the wave vectors for the incident and the scattered light. In our case every scatterer has this Doppler phenomenon, but the directions of the movements do not matter. Because of the complexity of the scattered light there has not yet been established accurate mathematical methods to describe this. However, the different wave vectors, velocity vectors and the multiple scattering all together may statistically be interpreted as a Doppler broadening of the scattered light [16]. A problem is that a part of the broadening is a pure random signal superposed with the Doppler broadening. A method to get rid of this noise is to measure the evolution of many speckles and use the mean value of them all. The random signals will then even out resulting in zero, for proof see further down about autocorrelation.

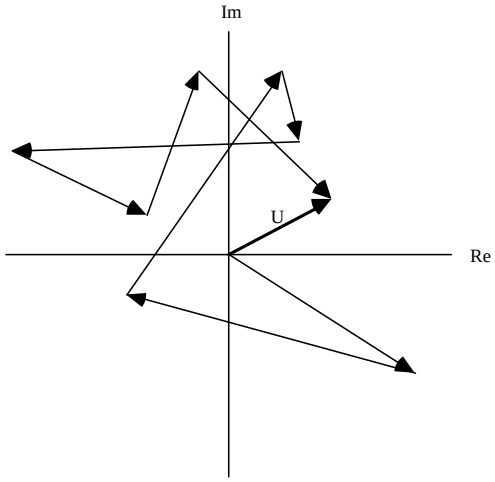

Figure 11. The complex sum of rays that create a spot in a speckle pattern .

2.2.3. Properties of biospeckles

In this work, the two most interesting dimensions of the speckles are size and intensity. The size of the stationary speckles are, as mentioned above, equal to the Airy disc resulting from the size of the illuminated area. But what happens with the size of the speckles as the light penetrates the object and is multiple scattered? Studies have been conducted to investigate the properties of time varying speckles. It has been shown that the speckles resulting from scattering inside an object have a smaller average size than the ones produced from scattering on the surface [4]. This can easily be explained with the expansion of the laser beam as it penetrates the object. As the light is scattered back, it leaves the object through a larger area than where it entered. In other words, the Airy law is still valid but with the actual size of the illuminated area rather than the width of the laser beam.

The speckle pattern is actually superposed of two different patterns. Large speckles, resulting from scattering on the surface and with a large angular dependence, are modulated by small speckles, from the light from the interior with very weak angular dependence [17]. In article [4], experiments with apples were made and the ratio of the sizes of the speckles was found to be 1:10. The same researcher showed with apertures that the speckle size increases with the decreasing diameter of the aperture and also that the rate of temporal changes of the speckles decreases with decreasing aperture size. The time varying effect of the speckles is also stronger far away from the direction of the specular reflection [4].

Another property that was found was the size of the region reached by light in the object when illuminating with a very thin laserbeam. It has the following dependence on the depth:

$$D = D_0\left[1 - \exp\left(-\frac{T}{T_0}\right)\right] \tag{7}$$

D is the diameter of the region and T is the depth. In the experiments with apples [4], D_0 = 20 mm and T_0 = 1.6 mm were empirically found, which give an illuminated area that can be illustrated like in figure 12. A depth of about 7 mm was found to be the maximum depth from where the scattered light contributes to the speckle pattern. It was discovered that the temporal speckle variations come mainly from scatterers within a few mm depth [4].

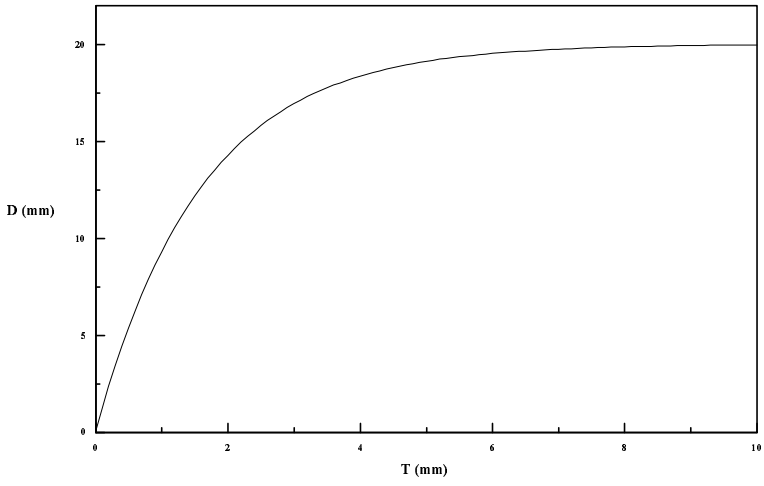

Figure 12. Diameter of region reached by light, D, as a function of depth in the matter, T.

The speckle is a stochastic effect and can therefore be described only statistically. There are many statistical approaches and several of them are evaluations from the concepts of first and second order statistics. The first order is the statistical description of the contrast of speckles in a pattern in one single image. This approach shows that the standard deviation, σ, of the spatial intensity is the mean intensity, $< I >$, of the

speckle pattern. The contrast may be expressed as $\frac{\sigma^2}{< I >^2}$ and when this ratio is 1, the pattern has a maximum contrast and is therefore fully developed [18]. This of course depends on the time the image is exposed. With a very long exposure, the image will become unclear, resulting in a very low contrast. However, with the knowledge of the time, the contrast and the ratio of moving scatterers to stationary ones, it is possible to determine the mean velocity of the scatterers. This technique can be used for example to visualise blood flow in the retina and to study vibrations [18].

The second order statistics is a description of the size and intensity distributions of the speckles in an image. The method involves taking the autocorrelation of the image to determine the sizes. This technique is also used to determine the changes of intensity in one single pixel by taking the autocorrelation of its time history. This latter technique will be used in this study and is therefore more thoroughly described further down.

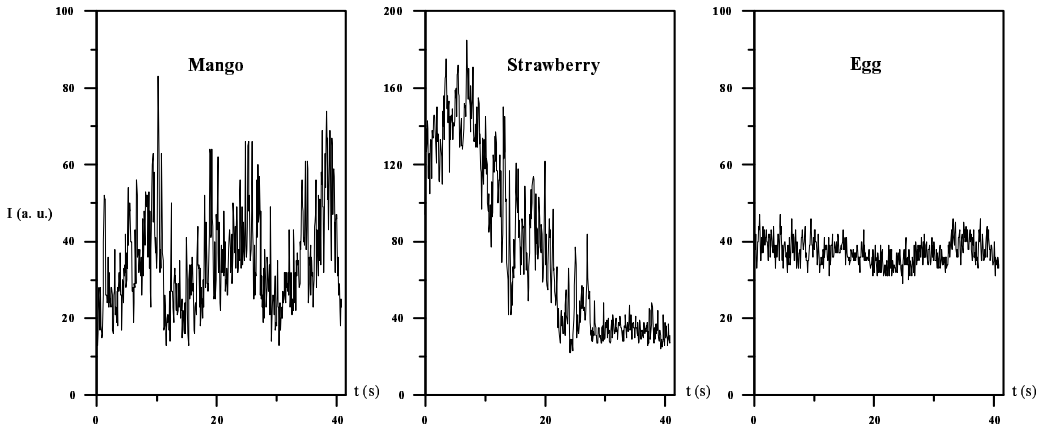

Figure 13. Time histories of speckles for different objects.

2.3. Autocorrelation and the Wiener-Khinchin theorem

A way of studying the evolution of speckles is to record the time history of its intensity. Figure 13 shows a typical time histories of speckles. In order to extract the information from the variations, it is common to take the autocorrelation of the time history, figure 14. The autocorrelation, $\gamma(t)$, is a technique to determine how the evolution correlates with itself [14];

$$\gamma(t) = \frac{1}{< I^2 >} \int_{-\infty}^{\infty} I(\tau) \cdot I(\tau - t) d\tau . \qquad (8)$$

I(t) is the time history function and $\frac{1}{< I^2 >}$ the normalising factor. For example, if a specific sequence of a variation appears a few times during the time history of the speckle, the autocorrelation will show a strong correlation for the entire duration of that sequence. After this sequence, the different parts of the time evolution will cross correlate with each other making the autocorrelation randomly stay around the mean value of the signal.

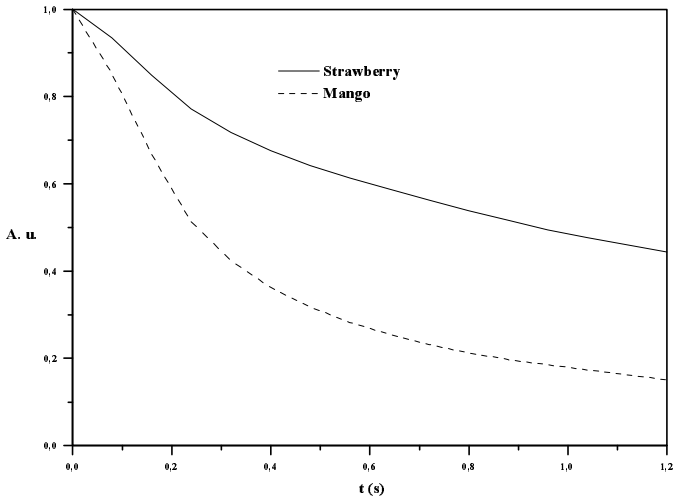

Figure 14. Autocorrelations of time histories of speckles for different objects.

As I have mentioned earlier, there is always a stationary speckle pattern that is superposed with the temporary evolution. To obtain only the fluctuations we subtract the mean value of the intensity. This means that we will have a time history that varies around the mean value zero and an autocorrelation that goes down to zero when the cross correlating begins. The correlation time, τ_c, can be defined as the time it takes for the normalised autocorrelation function to drop to for example 1/e or 1/2 of maximum. The smaller the value τ_c is, the faster the movement in the speckle pattern is.

As we can see there is a relation between the velocity of the scatterers and the correlation of their time history. The connection is defined by the Wiener-Khinchin theorem. This theorem enables us to study the quality of light, by transforming the normalised autocorrelation to show the power spectra of the signals that create the speckles. It is apparent that the autocorrelation function and the power spectral density, $P(\nu)$, form a Fourier transform pair [19]:

$$P(\nu) = \int_{-\infty}^{\infty} \gamma(\tau) \exp(-j2\pi\nu\tau) d\tau \tag{9}$$

$$\gamma(\tau) = \int_{-\infty}^{\infty} P(\nu) \exp(j2\pi\nu\tau) d\nu \tag{10}$$

The Fourier transform consists of a real part and an imaginary part. The transform of the function $f(\tau) = \gamma(\tau) + jw(\tau)$ is then

$$\begin{aligned} P(\nu) = & \int_{-\infty}^{\infty} \gamma(\tau) \cos(2\pi\nu\tau) d\tau + \int_{-\infty}^{\infty} w(\tau) \sin(2\pi\nu\tau) d\tau \\ & + j\left[\int_{-\infty}^{\infty} w(\tau) \cos(2\pi\nu\tau) d\tau - \int_{-\infty}^{\infty} \gamma(\tau) \sin(2\pi\nu\tau) d\tau \right] \end{aligned} \tag{11}$$

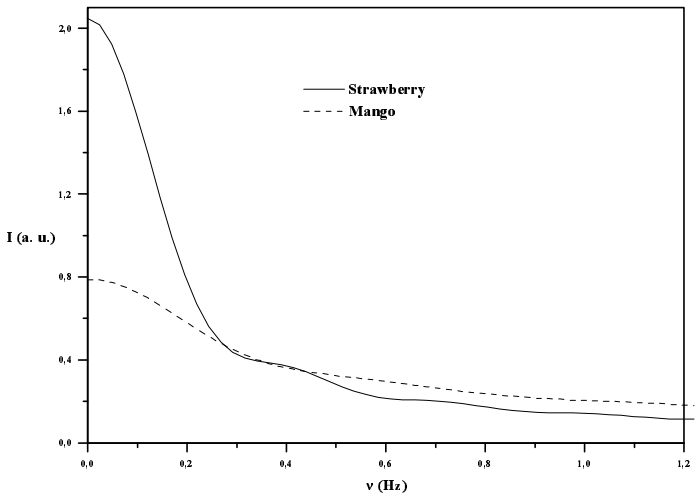

Figure 15. Fourier transforms of autocorrelations for different objects .

Since the autocorrelation only has a real part and is an even function, the Fourier transform will also be a real function and we will end up with [20]

$$P(\nu) = \int_{-\infty}^{\infty} \gamma(\tau)\cos(2\pi\nu\tau)d\tau = 2 \cdot \int_{0}^{\infty} \gamma(\tau)\cos(2\pi\nu\tau)d\tau \qquad (12)$$

This means that we can work with half the functions all the time, which saves a lot of space. There will always be an imaginary part in the calculations, it can hence be ignored.

Figures 14 and 15 show the autocorrelations and their Fourier transforms of images from three different fruits. As we can see, a short correlation time is the result of fast changes in the speckle pattern and hence a high frequency in the Fourier transform. From the power function we can extract the mean velocity of the scatterers with

$$|v| = \frac{\Delta\omega}{2}\left(\frac{1}{w} + \frac{\sigma^2}{\Delta x^2}\right)^{-1/2} = \frac{1}{\tau_c}\left(\frac{1}{w} + \frac{\sigma^2}{\Delta x^2}\right)^{-1/2} \qquad (13)$$

where $\Delta\omega$ is the width of the power spectra which obviously is proportional to v. The proportionality constant is related to the size of the speckles Δx and the illumination conditions with the parameters w and σ where $\sigma = \frac{R}{\rho} + 1$. w and ρ are the width and the wavefront-curvature radius of the beam at the object plane and R is the distance between the object and the distance plane [21], figure 16. In the experiments with strawberries the illumination conditions are the following; $\Delta x \approx 26\ \mu m$, $w \approx 2$ mm, R = 10 cm, and $\rho < 0.7$ m. $\Delta\omega$ = FWHM turns out to be approximately 0.2 Hz, figure 28, which makes $|v| \approx 2\ \mu m/s$.

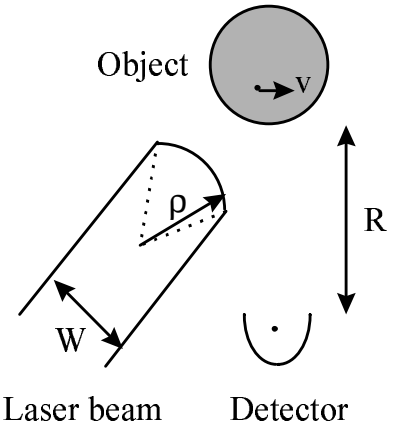

Figure 16. Different variables that effect the measurements of velocity.

Of course there will be random noise in the measurements of the time history, that will join the information through the autocorrelation and the transform and finally interfere with the values of the power spectra and the velocities. A way of getting rid of this is to simultaneously record the evolution of many speckles and take the mean value of all

the autocorrelations. For example one can use an array of 512 pixels as I have done in this study. An example of such an intensity evolution is shown in figure 17. This will level the noise to a zero everywhere in the autocorrelation except for t=0.

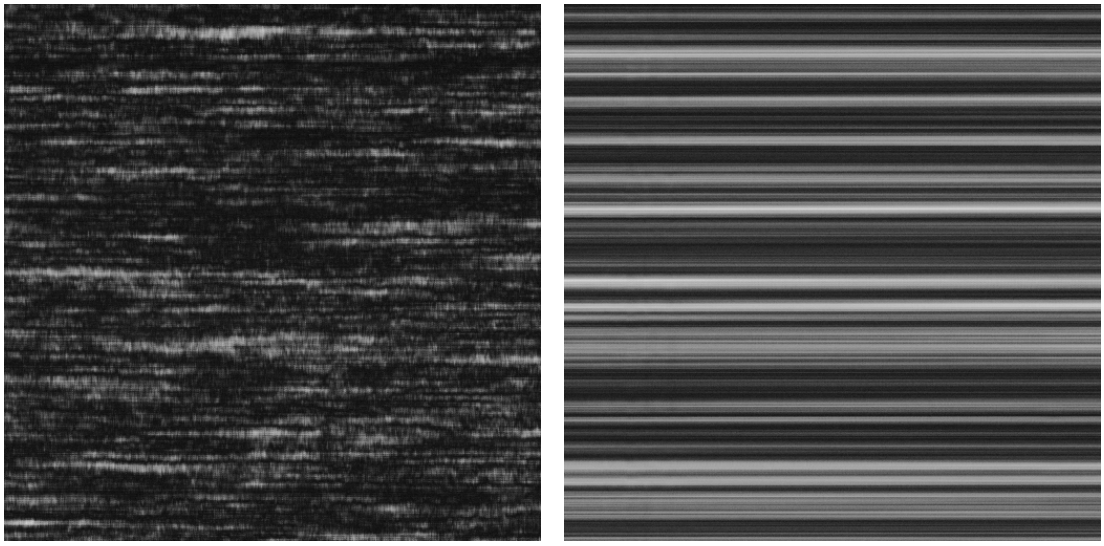

Figure 17. Images of 512 timehistories each, when measuring a strawberry (left) and a dead object (right).

To prove this, we calculate the effect of random noise in the autocorrelation of a time history. The time history of every pixel has changing intensity, I, at any given time (Any single frame taken by the image processor) decided by the activity in the speckle intensity $\hat{I}$, modulated by the random intensity $I(t)-\hat{I}$:

$$\begin{aligned} A(t) &= \left(I_1(t)-\hat{I}_1\right)\otimes\left(I_2(t)-\hat{I}_2\right)= \\ &I_1(t)\otimes I_2(t)-I_1(t)\otimes\hat{I}_2-\hat{I}_1\otimes I_2(t)+\hat{I}_1\otimes\hat{I}_2 \end{aligned} \tag{14}$$

In order to perform this autocorrelation we must take a few relations into consideration:

$I_1(t)$ and $I_2(t)$ are two random intensities which therefore are independent:

$$P\left(I_1\middle|I_2\right)=P(I_1). \tag{15}$$

The central correlation is expressed as follows:

$$C(I_1, I_2) = \left\langle \left(I_1 - \hat{I}_1\right)\left(I_2, \hat{I}_2\right)\right\rangle = \begin{cases} \sigma \cdot \delta(I_1 - I_2); \text{when: } I_1 = I_2 \\ 0; \text{when: } I_1 \neq I_2 \end{cases} \tag{16}$$

Let us now express every mean value of a time history of a pixel in the speckle pattern as a constant times the window. The window is a rectangle that lasts as long as the pixel is measured, a time constant here denoted b:

$$\hat{I}(t) = \hat{I} \cdot \text{rect}\left(\frac{t}{b}\right). \tag{17}$$

We then find that the autocorrelation above can be expressed as:

$$\begin{aligned} A(t) = I_1(t) \otimes I_2(t) - \hat{I}_2\left(I_1(t) \otimes \text{rect}\left(\frac{t}{b}\right)\right) \\ -\hat{I}_1\left(I_2(t) \otimes \text{rect}\left(\frac{t}{b}\right)\right) + \hat{I}_1 \cdot \hat{I}_2 \cdot \left(\text{rect}\left(\frac{t}{b}\right) \otimes \text{rect}\left(\frac{t}{b}\right)\right) \end{aligned} \tag{18}$$

In the processing of the image, we take the mean value of 512 autocorrelations:

$$\begin{aligned} \hat{A}(t) = < I_1(t) \otimes I_2(t) > - \hat{I}_1 \cdot \hat{I}_2 \cdot \left(\text{rect}\left(\frac{t}{b}\right) \otimes \text{rect}\left(\frac{t}{b}\right)\right) \\ -\hat{I}_1 \cdot \hat{I}_2 \cdot \left(\text{rect}\left(\frac{t}{b}\right) \otimes \text{rect}\left(\frac{t}{b}\right)\right) + \hat{I}_1 \cdot \hat{I}_2 \cdot \left(\text{rect}\left(\frac{t}{b}\right) \otimes \text{rect}\left(\frac{t}{b}\right)\right) \end{aligned} \tag{19}$$

According to the central correlation, this is zero everywhere except when $I_1 = I_2$. This gives us

$$< I_1(t) \otimes I_2(t) > = \hat{I}_1 \cdot \hat{I}_2 \cdot \left(\text{rect}\left(\frac{t}{b}\right) \otimes \text{rect}\left(\frac{t}{b}\right)\right) \tag{20}$$

which shows that the mean value of many autocorrelations of the total signal is the mean value of the signal without noise. However one detail remains. In A(0) we will obtain a peak which contains the total signal including noise.

$$\sigma \cdot \delta(0) = < I^2(0) > - \hat{I}^2 \tag{21}$$

Since the mean intensity in these experiments is subtracted from the measured values, this leaves us with the autocorrelation function $\gamma_{tot}(t) = \gamma(t) + \sigma \cdot \delta(t)$. The Fourier transform is then $P_{tot}(\nu) = P(\nu) + \sigma$ which means that there will always be a small constant bias due to noise in the power spectra. The size of the constant, $\sigma = < I_n^2 >$, will be studied further down, when discussing the limits of the equipment.

2.4. The line profile and its origin

The variations of the speckles depend, as I mentioned earlier, on the phase changes of the many different rays of light that compose it. The probability of the different phases is a rectangle function and does therefore not effect the shape of the line width [22]. Many of the rays are superposed and if there is a convolution it may be hard to distinguish different line shapes from each other. For instance, different gaussian shapes combine their widths, making another gaussian one. On the other hand, when working with autocorrelations and Fourier transform, it is beneficial to use the following property of the convolution [20]:

$$\int_{-\infty}^{\infty} G(\alpha)\cdot H(\nu-\alpha)d\alpha = G(\nu)*H(\nu) = F\big(g(t)\cdot h(t)\big) \qquad (22)$$

In other words, a convolution in the frequency domain is a product in the time domain. The most dominant effects that create the line profile are Doppler, Turbulence and Diffusion. In order to understand the changes in the line profile, those effects are described below:

2.4.1. The Doppler effect

The frequency of photons scattered from moving particles will be modified depending on the speed of the moving parts. An illustration of the effect is the sound of the cars on the highway changing in frequency between coming towards you and going away from you. This is called the Doppler effect, which is closely related to the process in the time varying speckles. However in the speckle pattern, the fluctuation is mainly caused by interference of many rays rather than shifts in single photons. According to the central limit theorem, independent stochastic variables have approximately a normal distribution as long as the number of trials is large. Assuming that the random movements of the many scatterers are independent, they obey the normal distribution and hence the Gaussian one [3].

Unlike the Doppler method, the direction of the movements of the scatterers are of no consequence to the speckle pattern. Both effects cause the same frequencies and broadenings and they both appear in the time varying speckles. The intensity fluctuation is however more dominated by the random phase variation due to interference than by the Doppler shift of photons, and therefore it is more correctly called time varying speckle phenomenon.

The measure I use for the Doppler width is the Full Width at Half Maximum (FWHM). Having determined this dimension it is easy to calculate the mean speed of the scatterers with equation 13. This mean value contains the broadenings from all types of scattering in all types of particles in the matter. Therefore small changes in one type of broadening may not even be noticeable in the resulting signal. In this study, I assume that the part of Doppler in the line shape is dominant and I therefore approximate the FWHM for Doppler broadening with FWHM for the results.

2.4.2. Turbulence

Turbulence is a problem for instance in astronomy and when studying the atmosphere optically. Warm and cold air have different refractive indexes, and differences in pressure changes the index as well. It is possible that a similar phenomenon exists in biological tissue. Several models have been created to statistically solve these kind of problems. In one model, Lee and Harp [22], the medium is imagined to consist of layers of temporally and randomly different refractive indexes. Every layer will shift the light a certain time varying phase, figure 18. The net optical phase in the detector is the sum over the individual phases ϕ_m;

$$\phi_{net} = \phi_1 + \phi_2 + \phi_3 + ... + \phi_n \qquad \text{with} \qquad \phi_m = n_m \cdot \Delta t_m \tag{23}$$

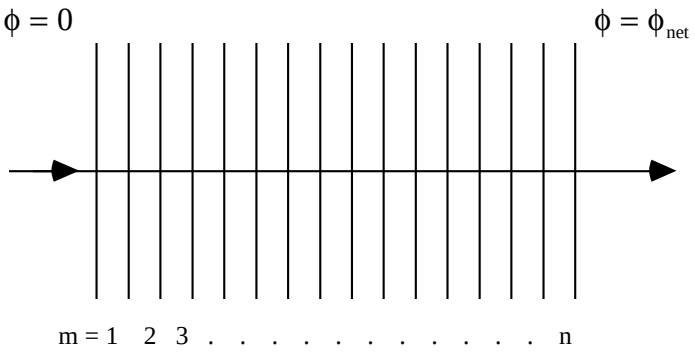

Figure 18. Turbulence changing the phase of the light.

where n_m is the random refractive index of the m:th plane with the random thickness Δt_m. Since the different planes act independently and the phase fluctuations within each plane obey the same physical laws, ϕ_{net} satisfies the central limit theory and is therefore normally distributed. The normal distribution has a Gaussian line shape and is therefore superposed with the Doppler broadening to another Gaussian one.

2.4.3. Diffusion

The fluids in and between the cells are mixtures of different liquids. They do not propagate but have fluctuations in density and concentration. The relaxation of these fluctuations is diffusive and has a time dependence $\exp(-\beta t)$. Like in any other matter the thermodynamics always oscillate around an equilibrium, and since the matter is alive, this process is continuous. In the scattered light it gives rise to broadened components centred at ν_0. This is clarified by the autocorrelation function for concentration fluctuations and isobaric density fluctuations of the wavevector $\bar{q}$ in fluids.

The return to the equilibrium concerning the concentration, C(t,r), is given by

$$\frac{\partial C}{\partial t} = D\nabla^2 C \tag{24}$$

where D is the diffusion coefficient.
The return to the equilibrium concerning the isobaric density, $\rho(t, r)$, is given by

$$\left(\frac{\partial \rho}{\partial t}\right)_p = \chi \nabla^2 \rho \tag{25}$$

where χ is the thermal diffusivity.
The autocorrelation functions for fluctuations of the wave vector $\bar{q}$ in fluids are then, according to [23],

$$\gamma_C(\tau) = < C_q{}^2 > \exp\left(-D \cdot q^2 |\tau|\right) \tag{26}$$

$$\gamma_\rho(\tau) = < \left|\rho_q\right|^2 > \exp\left(-\chi \cdot q^2 |\tau|\right) \tag{27}$$

The Fourier transform of an $\exp(-\beta\tau)$ is $\frac{\beta}{\beta^2 + \nu^2}$ which is a Lorentzian line shape. This will hence be the result of the fluctuations in concentration and density in the object. Of course there will be many different diffusions in biological tissue, resulting in a series of Lorentzians with different line widths all centred at ν_0 with an added total line width. A convolution between them is an addition of their diffusion constants in the autocorrelation.

2.4.4. The Voight profile

In a lot of optic and spectroscopy research one encounters the Voight profile. This profile is a convolution of a Gaussian line shape and a Lorentzian line shape. One can think of it as if every single Doppler-element were smeared out into a Lorentzian profile. Actually there are usually several different Lorentzian and Gaussian contributions to the shape. The Lorentzian for instance is normally a combination of pressure broadening and natural broadening. The resulting Lorentzian width of many contributions result in

$$\delta\nu_L = \delta\nu_{L1} + \delta\nu_{L2} + \ldots + \delta\nu_{LN}. \tag{28}$$

The corresponding relation for the Gaussian line shape, when several velocity shifts with different speed combines, is [24]

$$(\delta\nu_D)^2 = (\delta\nu_{D1})^2 + (\delta\nu_{D2})^2 + \ldots + (\delta\nu_{DN})^2 . \quad (29)$$

The greatest difference between the two shapes is that the Lorentzian profile has wider wings than the Gaussian one. This results in that the wings of the Voight profile almost entirely are decided by the Lorentzian, irrespective of its contribution. For example, at the double FWHM only 0,2 % of the Gaussian peak is represented compared to 6 % of the Lorentzian peak [24]. On the other hand, the central part and the FWHM of the line profile are almost entirely determined by the Gaussian contribution. This fact is used when calculating the ratio of Lorentzian to Gaussian width ($y_{L/D}$)

Optical transfer in the atmosphere is an example of when the Voight profile can be applied. At sea level the line shape is almost pure Lorentzian but 30 km up in the air the relationship is 50/50. In this case the Lorentzian shape is pressure dependent and the Gaussian one depends on the Doppler shift of the radiators, in other words the temperature [25]. Another example is when working with plasma waves and acoustics in astrophysics. The mathematical functions describing the profile is in this case the same as in the atmosphere but the physical reasons are different.

The definition of the Voight profile is given by equation 30 [25]:

$$P(x,y) = \frac{1}{\alpha_D}\sqrt{\frac{\ln 2}{\pi}} \cdot K(x,y) \quad (30)$$

where $K(x,y)$ is called the Voight function and is given by:

$$K(x,y) = \frac{y}{\pi}\int_{-\infty}^{\infty} \frac{\exp(-t^2)}{y^2 + (x-t)^2} dt \quad (31)$$

where:

$$y_{L/D} = \frac{\alpha_L}{\alpha_D}\sqrt{\ln 2} \qquad \text{(ratio of Lorentzian to Gaussian width)} \quad (32)$$

$$x = \frac{\nu - \nu_0}{\alpha_D}\sqrt{\ln 2} \qquad \text{(wave number scale in units of Gaussian width)} \quad (33)$$

$$\alpha_D = \nu_0\sqrt{\frac{2kT\ln 2}{Mc^2}} \qquad \text{(Gaussian half width)} \quad (34)$$

α_L is the Lorentzian half width, M is the atomic weight, ν_0 is the wave number of the line centre and ν is the wave number at which K(x,y) is to be evaluated. Equation 30 is that of a probability distribution where P is normalised to unity on $(\nu - \nu_0)$. But equation 31 will be used in this study to describe the Voight function since the

difference between the equations 30 and 31 at a given Gaussian width is only a constant. Figure 19 shows K(x,y) as a function of x for some different values of $y_{L/D}$. The graphs are normalised to contain the same total amount of intensity $I(\nu)$

$$\int_{-\infty}^{\infty} I(\nu)d\nu = 100. \tag{35}$$

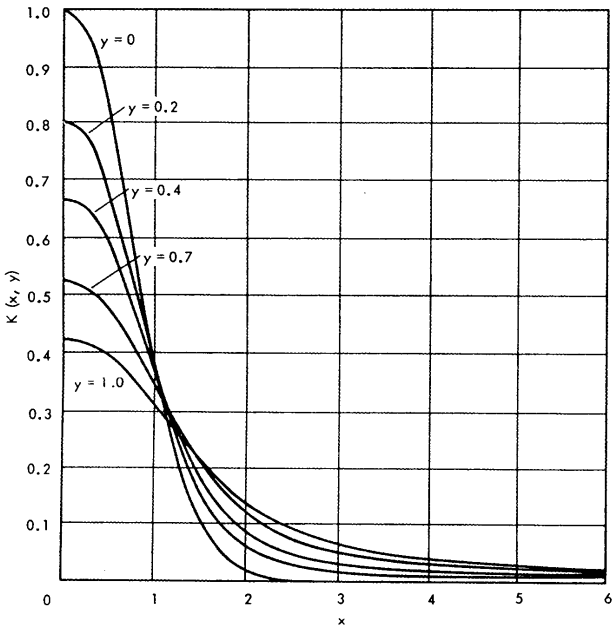

Figure 19. The Voight function for different values of $y_{L/D}$ [25].

When y=0, the line shape is pure Gaussian and when it is infinitely large, it is a pure Lorentzian. Everything with a similar shape in-between these two extremes is a Voight. As we can see, when the Gaussian profile is dominant, the FWHM does not change very much with $y_{L/D}$. The FWHM will therefore be used as a measure, of the size of the Doppler broadening in the signal. The height of the probability function, when x >> FWHM and x << FWHM, changes with $y_{L/D}$ and this may be used to determine the amount of Lorentzian shape in the profile. To be able to compare the different profiles it is necessary to initially re-scale the x-axis of all the profiles and then normalise the total intensity according to equation 35.

2.4.5. Other broadenings and shifts

The line shape is not only dependent on the different broadenings but also on different shifts and inelastic scattering effects which interfere with the elastically scattered light. The large shifts do not effect the measurements in this study because they change faster than the slow speed of the equipment. The time that elapses between the recording of two frames of images is 80 ms. This means that the highest frequency that will be measurable is $\frac{1}{0.080}$ s^{-1} =12.5 Hz, which corresponds to $\frac{f}{c}\cdot 10^{-2} = \frac{12.5}{3\cdot 10^{8}}\cdot 10^{-2}$ cm^{-1} = $4\cdot 10^{-10}$ cm^{-1}. Everything that changes with a higher rate, or has a bigger shift or broadening, will be recorded as random noise. Therefore the Raman scattering which normally has shifts between 100-1000 cm^{-1} [21] is not noticeable. Even if it would have had small shifts, the cross section for Raman is very small, one million times smaller than for fluorescence, and is therefore not detectable in this study anyway.

Fluorescence of absorbed energy may be of the same frequency but has a delay in the ns region. That is about the time it takes for the wave package to pass as a whole, keeping the waves from interfering with each other apart from randomly. The Brillouin-scattering is probably one of the most important effects that will disturb the measurements. Acoustic waves with a frequency of a few hertz will not be audible with the human ear but may vibrate the setup. Let us imagine a very rough model of the object, a 3 cm wide crystal consisting of proteins. An estimation of the lowest phonon frequency possible in the object is $\nu = \frac{v_o}{\lambda} = \frac{10^3}{3\cdot 10^{-2}}$ = 33 kHz, where v_o is the approximate velocity of sound in the object, which is a far too high frequency to be noticeable in this work. Lower frequencies will show as displacements of the object unless if the detector moves with it. The setup as a whole may however have resonance frequencies in the region of our measurements. These vibrations and displacements may be transmitted from the building through the ground or the air. The walls and floors of a building undergo mostly shear and bending vibrations which usually resonate at frequencies between 15 and 25 Hz. The buildings may transfer or be excited by vibrations from for example machines with frequencies typically between 10 and 100 Hz, ventilation ducts typically between 6 and 65 Hz and people walking and working in laboratories typically in the range of 1 to 3 Hz [26]. Typical floor vibration amplitudes are between 10^{-7} and 10^{-6} m [27] which is about ten times larger than the wavelength used in this work and therefore of great importance.

Raman scattering and fluorescence will not greatly influence the measurements. If the experiments were combined with spectroscopy one would probably be able to extract more information because of all the shifts that are specific for the object. However, considering the level of this study, should these factors interfere, they will only be noise among the broadenings due to Doppler, index shift and diffusion. The Brillouin-scattering, however, is obviously the most important source of noise in this work and need to be considered when evaluating the results of the measurements.

2.5. The development of strawberries

The development of strawberries is very unusual because they, unlike most other fruits, continue to increase in weight throughout the development including the ripening. Furthermore, the developing process of strawberries is visually apparent. They change in colour, softness and flavour as well as in size. The whole process lasts for only a few weeks depending strongly on the environment, especially the temperature. The ripening part happens fast with a very short time of optimum condition of the fruits. The definitions of the different stages that have been used among researchers, and for the sake of continuity also will be used here, are: small green (SG), large green (LG), white (W), pink (P), red (R) and dark red (DR) [28,29,30]. Since the development is a relatively fast process, the different phases may overlap, making the studies of them more difficult.

The initial growth after petal fall is due to a combination of cell division and cell expansion. After about a week, the cell multiplication is completed and replaced by a period of growth during which the cells only increases in volume. The expansion is influenced by the turgor pressure and correlates with concentration of solutes including sugar [31]. The strawberry grows to a size according to the number of cells that have been created at first. Which size the strawberry finally reaches, depends on genetic factors and is correlated with the number of seeds it has.

	Sugar content (mg/g fresh weight)				**Sugar flow (μg/min)**	
Stage	Free space	Cytoplasm	Vacuole	Total	P M	T P
Large green	5.7 ± 0.3	4.0 ± 0.4	35.2 ± 0.9	44.8 ± 1.6	487 ± 8	293 ± 45
Pink	10.0 ± 0.1	12.1 ± 1.6	52.9 ± 4.0	75.0 ± 5.7	570 ± 4	84 ± 5

Table 1. Sugar content in cells and sugar flow through cellular membranes at two stages of the development of strawberries. P M is the plasma membrane and T P the tonoplast, which is the membrane around the vacuole [31].

As the cell enlarges, it is accompanied by major changes in the cell wall and the sub cellular structure. At petal fall the cells have dens walls and small vacuoles. When growing, the disorganisation increases and the fruit obtains a softer structure. The softening process, as well as the post harvest shelf life, depend very much on the change of the cell walls. Therefore this has been extensively studied [28,29]. Nevertheless, researchers still do not agree on what causes the degradation of the cell wall. It is for certain though, that the wall composition changes as it grows. It alternates polymers which results in an overall increase in the proportion of low molecular weight polymers [28]. This makes the tissue unable to maintain its structural

integrity since the components of the wall are less tightly bound. When the cell finally breaks, the contents of the vacuole smear out between all the other cells making the tissue even softer.

Sugar is needed to provide energy for the metabolic changes that constantly occur. Sucrose, glucose and fructose constitutes 99 % of all the sugar in the fruit, 83 % being glucose and fructose [30]. The process of sugar accumulation is still poorly understood but it more or less diffuses through the strawberry to reach every cell. It is known that the sugar composition varies with the degree of ripeness. The growth rate of the strawberry actually correlates with the sugar uptake. Most of the imported sugar accumulates in the vacuole which contains more than 70 % of the total amount of sugar [31]. Table 1 shows the sugar content and velocity through membranes at two different stages of the development. It is evident that the flow of sugar through the tonoplast into the vacuole is higher as the strawberry is green. As the strawberry turns red however, the cells break and cause a strong flow of subparts of cells, including sugar.

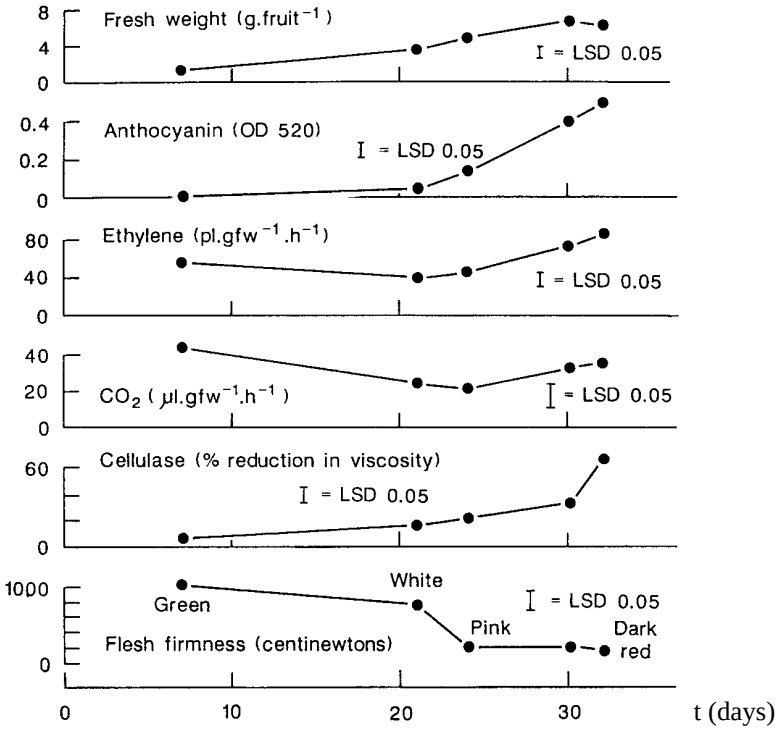

Figure 20. Physical changes of strawberries at different stages of the development [30].

Acids regulate the pH value and may influence the appearance of fruit pigment. The pigment characteristics are constantly changing with degradation of existing ones and synthesis of new ones. The most obvious change is the destruction of chlorophyll. It is consistent with the disappearance of chloroplasts and decrease in contents of carotenoids. The strawberry actually imports most if its energy from the plant, but in its initial stages of development it needs extra energy to multiply its cells. During this phase it therefore contains chlorophyll and complements the import with its own

photosynthesis. Finally the strawberry turns red in order to attract animals to eat it, and thereby spread the seeds.

All these changes in the strawberry; the different movements of cells and the various subparts, the changes in colours and the diffusion of sugar, water and cell shape during the development may influence the interaction with light. An important change should for instance appear as the cells brake and the vacuoles start to leak. The effects it may have on the signal is described above in chapter 2.4. The changes in some of the different stages can be seen in figure 20.

3. Experimental study

3.1. Introduction

The objective of the experimental work was to find a relationship between the signals, obtained from the scattered light, and the changes in the process of maturing fruit. The equipment was investigated and optimised in order to find the limits of the experiments and the possibility of stretching them. Before the real measurements started, it was necessary to find out which fruits were suitable enough to measure. It was also interesting to study how the signals differ with the different macroscopic characteristics of fruits. A great number of fruits, with different characteristics, were therefore measured. The strawberry turned out to be a suitable fruit for the measurements of maturation for many reasons. Bearing in mind that the maturation process of the strawberry is very fast, the activity was not too fast to register. The obvious visible changes of the strawberry that occur and reveal the stage of maturation are also very important. Furthermore, the small potted strawberry plants are easy to carry in and out of the laboratory. Two experimental setups were used. The first one, called setup A, was used during the experiments with different fruits and pilot tests of three strawberries. The second setup, called setup B, was used during the experiments of the rest of the strawberries as well as the tests of the equipment.

3.2. The experimental setup and equipment

3.2.1. Setup A: With an expanded laser beam and without a diaphragm.

The setup is illustrated in figure 21. The camera is focused on the surface of the object. To fill the whole image with a speckle pattern, diameter 10 mm, the laser beam is expanded with a lens. This setup did however turn out to have some characteristics which could be improved. It was hard to be in control of the focusing as the surfaces of the fruits never were completely even and the intensity distribution on the surface was not constant. Due to the curvature of the object it is also hard to control the angle of incident and reflected light. The speckle size also varied with the depth of the penetration of light and were always very small. Setup A was therefore exchanged for setup B after the experiments with different fruits and a pilot test with three strawberries.

3.2.2. Setup B: With a normal laser beam and with a diaphragm.

This setup is illustrated in figure 22. The changes compared to setup A is that the laser beam is not expanded and there is a diaphragm with diameter 2 mm in front of the object which is a size close to the diameter of the laser beam. This makes it possible to control the size of the speckles and limit the detection of light scattered deep into the tissue, without limiting the intensity of incoming light. The camera now has an extension on the objective enabling it to focus very close to the camera lens. The image on this plane in front of the camera consists of a pattern of large speckles, all

arisen from approximately the same area of the object. The mean diameter of the speckles in setup B is, according to Airy:

$$d = 2 \cdot 1.22\left(\frac{\lambda \cdot z}{D}\right) = 2 \cdot 1.22\left(\frac{633 \cdot 10^{-9} \cdot 0.10}{3 \cdot 10^{-3}}\right) m = 77\ \mu m \qquad (36)$$

This is about ten times bigger than a pixel in the camera, which limits the risk of detecting more than one speckle in one pixel.

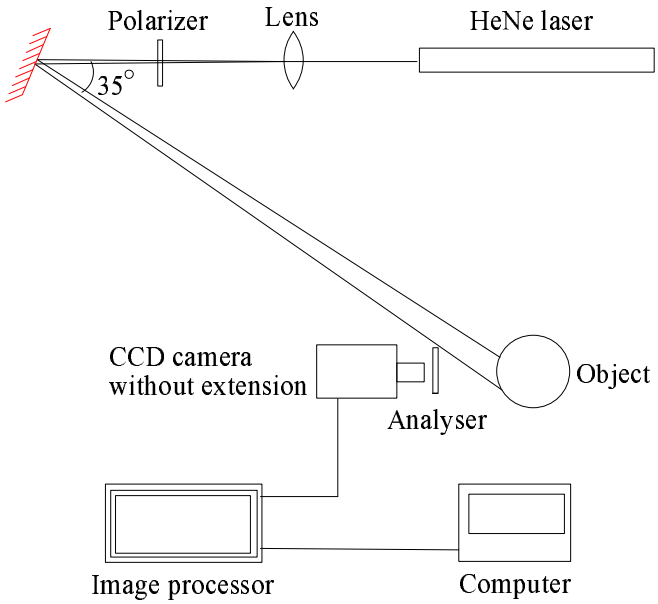

Figure 21. Setup A.

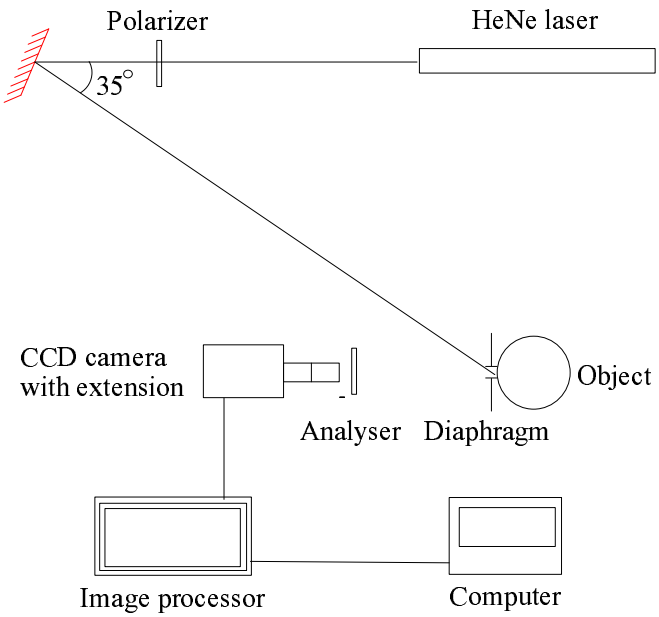

Figure 22. Setup B.

3.2.3. Equipment

The laser is a 632.8 nm HeNe-laser with an output of 10 mW single mode TEM_{00}. It comes from Melles Griot and is called 05-LHP-991. It has an angular drift of less than 0.03 mrad after 15 min and a noise amplitude of less than 0.5 %.

The camera is a PULNIX TM-560 No 010038. It has a detection plate that consists of 512 x 512 pixels. The lens has the f number 1:1.4, the diameter 16 mm and the outer diameter 25.5 mm. The lens is extended with a 40 mm COSMICAR TV-lens extension tube in setup B. The camera sends images to the image processor at a maximum rate of 50 Hz.

The image processor is an ADI-151 from Imaging Technology Inc. It digitises incoming imagery from video inputs and stores it momentarily in two sets of archives (512 x 512). It has a signal-to-noise ratio greater than 40 dB. When testing the speed of the grabbing, it was acknowledged that the processor registers frames at 12.5 Hz which therefore is the highest frequency that can be detected. The program, ATO12.C, was modified to register only a few pixels of the image from the camera to make the processor faster. However it turns out that it is necessary to skip many pixels so as to get a higher rate of registration. The loss of accuracy due to fewer pixels is for this reason not worth the small increase in frequency of the registration. This modification was therefore not used in the final ATO12.C. Since the time history of a pixel is recorded during 512*80.2 ms = 41 s, the lowest frequency that will be recorded is 24 mHz.

3.2.4. Computer programs

Many different computer programs were used in the many pilot tests performed during the course of the experimental study. I will however only mention the most important ones:

ATO12.C is the name of the program that controls the image processor and stores the images in the computer. It was written at CIOp a few years ago and works well with the rest of the equipment.

GRABA.C takes as snapshot of the image in the camera.

VOIGHT.FOR is used to calculate Voight profiles. The input is a file of x-values and the output is a file of $y_{L/D}$-values thus forming the profile. It can be found in [25].

FRUTY.C is a program that removes the head from the image file, subtracts the mean value of the time history of each pixel, autocorrelates the 512 time histories and takes the mean autocorrelation of them all as well as Fourier transforms the autocorrelation. The following data is obtained for every image:
- files of autocorrelation,
- Fourier transform,

- re-scaled x-values for the power spectra to normalise it to be comparable with the Voight profile,
- FWHM,
- $y_{L/D}$ (importance of Lorentzian shape in the profile compared to the Gaussian),
- mean value of the time histories and
- $< I^2(0) >$.

This program was written by the author and includes sections from other programs written at CIOp. FRUTY.C is printed in the appendix.

TOMY22.C is a forerunner to FRUTY.C which performs similar calculations apart from calculating the Fourier transform. In stead of FWHM, it gives the correlation time of the autocorrelation.

3.3. Experimental procedure

Seeing that the setups were very sensible, they had to be treated with the utmost caution throughout the experiments. Firstly, I always turned the laser on about an hour prior to it being used. This was to ensure stability of the laser beam. A change or fluctuation in intensity would influence the scattered light from the whole object and the autocorrelation would identify it as a consistent signal and therefore not dismiss it as noise. The same thing would happen if there were external shocks on the object. For this reason I was quiet and kept still during the measurements. Of course, I always turned off all the lights in the laboratory and the chinks by the door were taped. The only light that was present, other than that from the laser, was from the computer screen and from the diodes on the rest of the electronic equipment.

The first step in the measurements was to;
Setup A: put the fruit in front of the camera, with the expanded beam in the centre of it, and focus the camera on the surface of the fruit.
Setup B: coincide the size of the diaphragm with the size of the laser beam diameter and place the strawberry right behind it.
Since I made two measurements with different polarisation's, of each object every time, I had to turn the analyser 90° between the two measurements. The data was recorded as the time history over 512 frames of 512 pixels in the speckle pattern. The program ATO12.C was used to collect the time evolved information from the image processor. The lapsed time between every frame was typically 80.2 ms. The images were stored in a computer and later processed with the program FRUTY.C. With the program GRABA.C, I could view an instant image and also record it. This enables to study first order statistics of the object.

At every measurement, the object was not illuminated more than necessary, in order to reduce possible injuries or induced heat on the surface of the object. On an average each measurement took about two minutes. The strawberries were measured once per day, and twice during periods of high cell activity i.e. when turning white, pink and red.

3.4. Study of noise

3.4.1. Introduction

When working with speckles there will always be random movements that do not add any information about the object but that will disappear in a mean value of many measurements. There will also be error due to fluctuations or movements due to the equipment and the surroundings. By estimating the source and amount of noise present in the measurements, it is possible to either reduce the noise producing factors or to estimate the reliability of the results. Tests were done with each and every part of the equipment. I simply added one part of the equipment after the other, and studied the amount of noise for each combination and determined if the noise was random or not. When checking the camera, it was covered with a thick black cloth to prevent any incoming light. The laser was kept off until the dead objects were about to be measured.

3.4.2. Results

Piece of equipment added to the setup	Correlation time (ms)	$< I^2(0) >$ (au)
Image processor (Impr1)	0	0
Cord Impr-Camera (Cord1)	0	0
Camera covered (Cam1)	1.02	1.76
Camera covered (Cam2)	1.02	1.75
Camera uncovered (Cam3)	1.02	1.75
Camera uncovered (Cam4)	1.01	1.74
Dead object (Dead1)	1.36	6.94
Dead object (Dead2)	1.05	2.69
Dead object (Dead3)	1.40	3.52
Dead object (Dead4)	1.04	1.49
Strawberry 1	18.21	310
Strawberry 2	16.88	306

Table 2. Noise depending on different parts of the equipment. The names in parenthesis are the names of the files of data.

Table 2 shows the different combinations that were measured and their respective correlation times and values of $< I^2(0) >$. The autocorrelations are also presented in a more pedagogical way in figure 23. As we can see there is no noise until the camera is connected. The measurements of absolute dead objects are also very similar to the ones for only the camera. It is hence obvious that most of the noise comes from the camera. Since the autocorrelation drops directly after the t = 0 and after that decreases linearly, the noise is fully random according to the proof mentioned earlier, equation 20. The height of the delta is the value of $< I^2(0) >$. This is to be compared with the values of $< I^2(0) >$ for the measurements of fruits. It turns out that the signal to noise ratio at t = 0 is about 1000, which is enough for what is necessary in this study. Furthermore, if the random noise is believed to have constant mean intensity it does

not effect the comparison between the measurements of different fruits or stages in the maturation of strawberries.

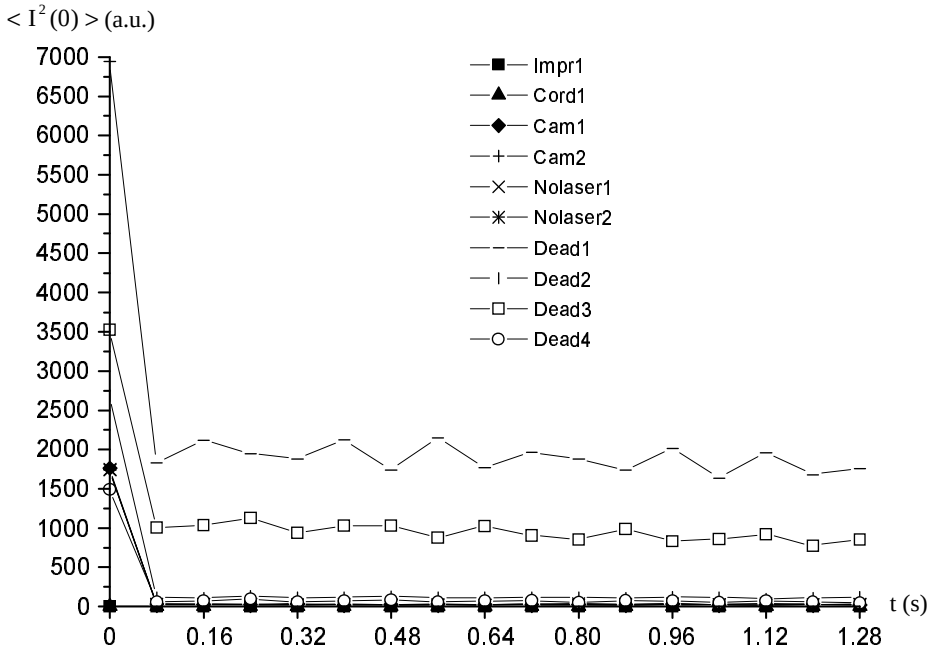

Figure 23. Autocorrelation of the time histories when measuring the noise.

The none random noise however, may be a factor to take into account. This can be seen in the measurements of dead objects which have a correlation time longer than that of the camera. It arises from disturbances that are uniform over the object, such as vibrations of the camera or the object, and Brillouin scattering due to acoustic waves in the object and setup. The vibrations may have their origin in people walking or closing doors in other parts of the building and are propagating through the walls and floors to finally be distributed to the setup. This external noise will hence not disappear in the mean autocorrelation and would therefore need an external detector to be noticed.

Another aspect that needs to be taken into account when working with CCD detectors is the shot noise. This type of noise fluctuates and may even appear as sparks in the detector. The result from such sparks is a rapid 12.5 Hz fluctuation, which is the highest measurable frequency, in the timehistory of a pixel in the camera. To eliminate this effect I filter the timehistories by using a procedure that for every value uses the median of itself and its two nearest neighbour values. This way I simultaneously get rid of the fluctuations of the pixels that are faster than 12.5 Hz, since these are detected as a 12.5 Hz signal with a random amplitude. To study the effect of the filtering I calculate the results from the different fruits with and without filter and compare the results, which are presented in table 3. Obviously there is no systematic factor in the results due to the filtering. This filter will be used in the studies of strawberries.

Fruit	FWHM (Hz)	FWHM with filter (Hz)	$y_{L/D}$	$y_{L/D}$ with filter
Pumpkin	0.365	0.365	1.013	1.038
Banana	0.365	0.365	0.971	0.973
Chirimoya	0.146	0.146	0.733	0.709
Egg	0.073	0.073	0.388	0.353
Lettuce	0.146	0.146	0.649	0.619
Mango	0.341	0.341	1.048	1.024

Table 3. Comparison between calculations with and without filter.

The effect the total noise has on the width of the Lorentzian shape is bigger than that on the FWHM of the Gaussian one, equations 28 and 29, which must be taken into account when evaluating the results of the measurements.

3.5. Study of the line profile of light scattered in different fruits and vegetables

3.5.1. Introduction

Fruits and vegetables with a wide variety of characteristics were selected. Some were with hard peel, some without peel, some containing a lot of water and all with different colours. They were all measured once with setup A. FRUTY.C was then used to calculate the FWHM of the line width and the amount of Lorentzian shape in the line profile, $y_{L/D}$.

3.5.2. Results

Table 3 shows the results from all the studied fruits and vegetables, and figure 24 shows the different line shapes. Since all the fruits and vegetables had different features and varying surfaces, problems with focusing occurred. Furthermore the camera would interpret features of some fruits as if they were speckles, for instance when measuring corn and avocado. The results are rather systematic and divide the objects into three major groups of similar results. The first consists mainly of fruits with thick peel; banana, mango, potato and pumpkin. The second group is mainly with hard peel; aubergine, avocado, chirimoya (and egg). The third group is the rest of the fruits; green/red apple, strawberry (and lettuce). In general, the FWHM is bigger when the analyser is perpendicular to the polariser since there is more activity inside the object than at its surface.

		Analyser perpendicular to polariser		**Analyser parallel with polariser**	
	Fruit	**FWHM (Hz)**	**$y_{L/D}$**	**FWHM (Hz)**	**$y_{L/D}$**
Thick peel	**Banana**	0.365	0.971	0.195	0.897
	Mango	0.341	1.048	0.219	0.918
	Potato	0.390	0.937	0.292	0.991
	Pumpkin	0.365	1.013	0.219	1.023
Hard peel	**Aubergine**	0.122	0.646	0.097	0.503
	Avocado	0.146	0.779	0.122	0.668
	Chirimoya	0.146	0.733	0.097	0.486
	Egg	0.073	0.388	0.049	1.704
Other	**Green apple**	0.244	0.889	0.170	0.873
	Lettuce	0.146	0.649	0.146	0.675
	Red apple	0.170	0.813	0.146	0.686
	Strawberry	0.170	0.894	0.170	0.745

Table 4. FWHM and $y_{L/D}$ obtained when measuring different fruits and vegetables.

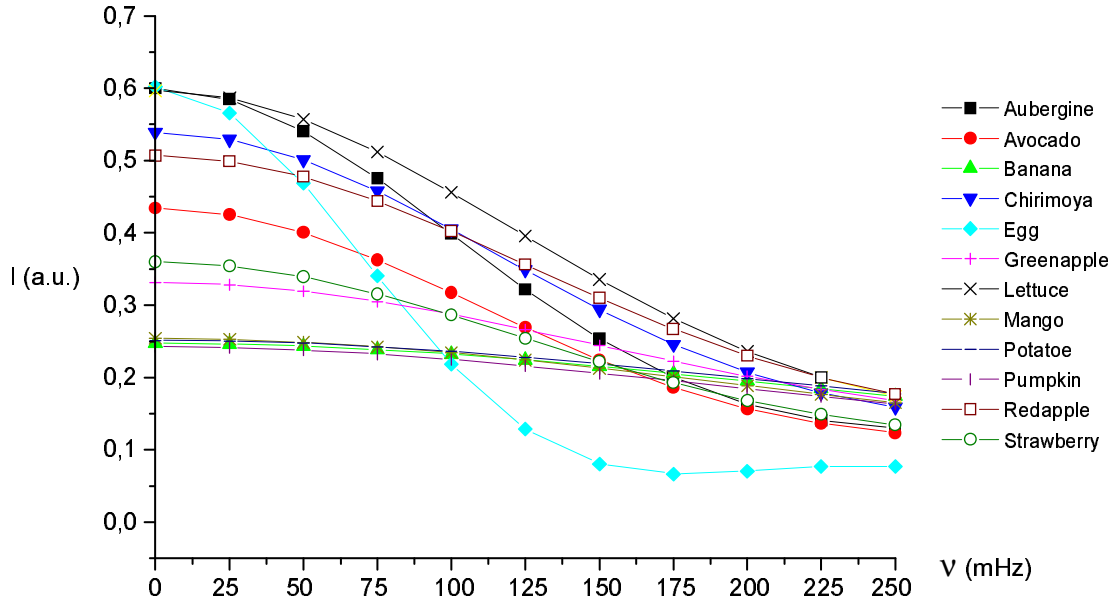

Figure 24. Line profiles from the measurements of different fruits and vegetables.

The fruits and vegetables with thick peel have typically big FWHM and $y_{L/D}$. They have also the biggest difference in FWHM when turning the analyser parallel to the polariser. The value goes down to 0.55-0.65 of the original value. Typical results for the fruits and vegetables with hard peel are small FWHM and $y_{L/D}$. These values also change when the analyser is turned. The FWHM goes down to 0.65-0.85 of the original value which is less than when measuring the objects with thick peel. An explanation for this phenomena may be that the light penetrates the objects with thick peel better than those with hard peel, and therefore show big variations between the interior and the surface of the object. The rest of the fruits and vegetables have values in-between the values for the two other groups but when the analyser is turned, their FWHM do not change very much. A reason for this may be that these fruits are soft enough to have almost the same activity inside as on the surface. Lettuce, having no peel and practically no depth, shows different results than the rest of the objects. Neither the FWHM nor the $y_{L/D}$ change much when turning the analyser.

The division into three different groups is however made mainly with respect to the FWHM. When evaluating the changes of $y_{L/D}$, it is clear that the diffusion increases for some of the objects and decreases for others, when turning the analyser parallel to the polariser. For vegetables such as pumpkin, potato, lettuce and egg $y_{L/D}$ increases, but for the fruits and some of the vegetables it decreases, especially chirimoya and aubergine. The vegetables obviously have such massive peels that the activity is interpreted as more diffusive on the surface than in or behind the peels. Both chirimoya and aubergine have rather hard peels, but apparently the light still penetrates them and returns with information about the diffusive activity inside the object, which is greater than that on the surface.

3.6. Study of the line profile of light scattered in strawberries during maturation

3.6.1. Introduction

Prior to the study, a test was made with three strawberries - ST1, ST2 and ST3 with setup A - to get an idea of the results and to discover difficulties. After this it was decided to change the setup from A to B. Two sets of strawberries were measured with setup B, where ST4, ST5 and ST6 belonged to the first set. When these three plants died due to the laboratory environment before fully maturing, it was necessary to measure additional plants in different stages, namely set two; ST7, ST8, ST9, ST10 and ST11. The stages of each strawberry can be seen in figure 25. The strawberries were measured normally once every day, but when they were about to change colours they were measured twice a day since that process is rapid. FRUTY.C was used to process the data. The activity studied with the analyser perpendicular to the polariser is referred to as internal activity, and with the analyser parallel external or surface activity.

3.6.2. Results

The results of the measurements are illustrated in figure 25. The time scale that is used is the maturity of the strawberries; small green, (large) green, white, pink, red or dark red, rather than time in days. The reason is that the speed of maturation differs very much from day to day which makes it very difficult to make comparisons between the strawberries based on days. The time axis is not linear because of this, hence some of the graphs are not according to scale, which must be taken into account when evaluating the results. As can be seen, the results are rather stochastic which probably depends on different kinds of noise and disturbances. However, there are some very interesting tendencies to recognise.

FWHM is around 0.1-0.3 Hz through all phases of maturation. The general tendency is that the FWHM is high when the strawberries are small green or red but low when they are white. This is especially evident in the results from the internal activity. As the strawberries turn red and dark red the results shift to a great extent and when they are white the results are rather constant. A possible explanation for the rapid changes is that the strawberries were measured twice a day after they had turned pink and hence may have had different conditions in the environment. Generally, the internal graphs are smother and higher than those from the movements on the surface. The results from the external activity have many high peaks at single measurements which makes them look rather stochastic. These peaks may be due to external disturbances, especially when they do not correlate with peaks in the internal measurements.

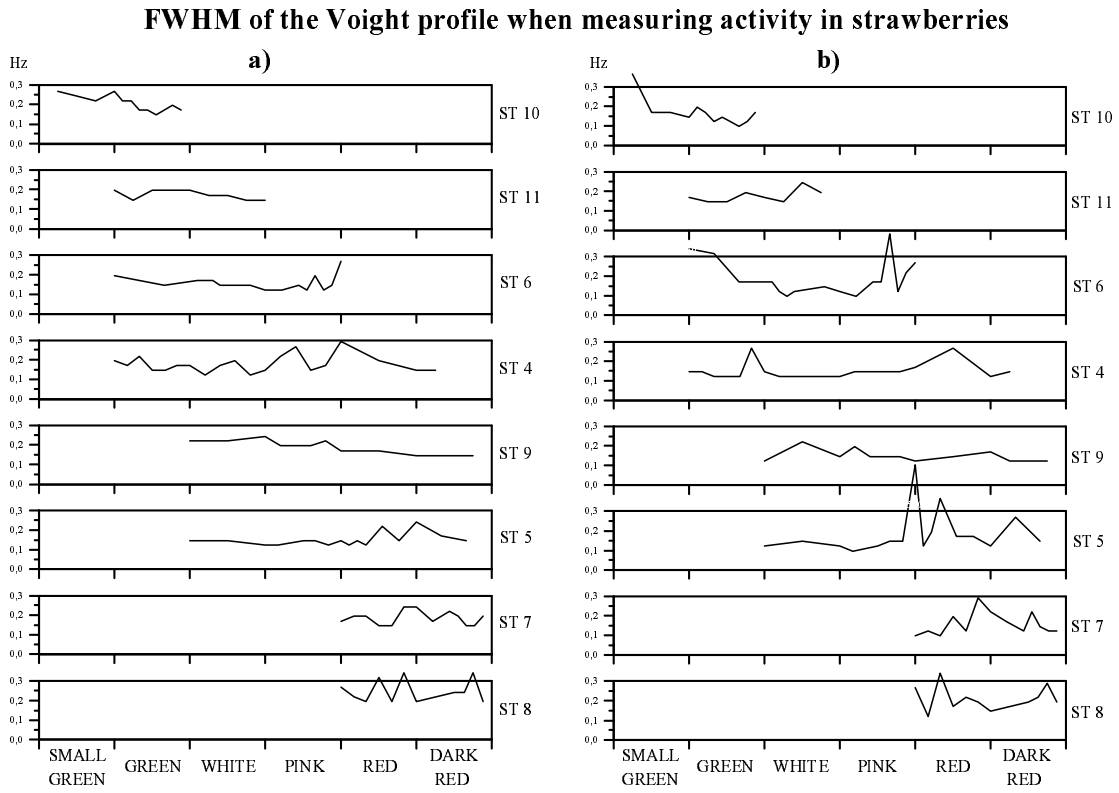

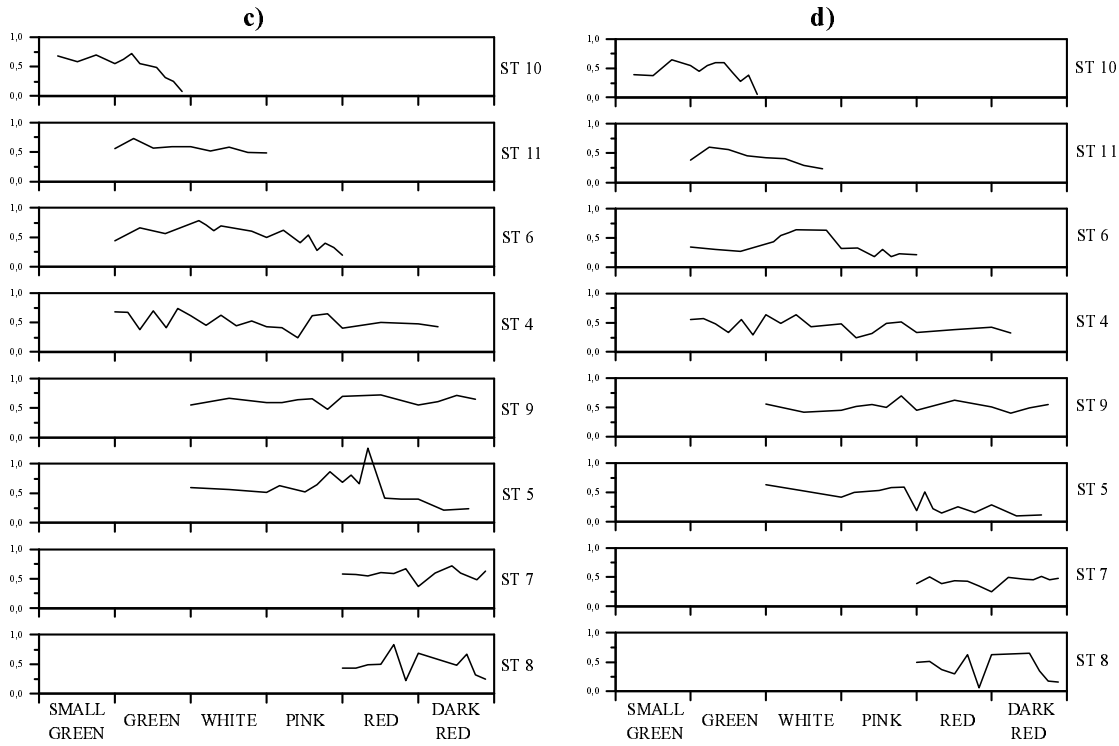

25. (a,c) Internal activity. **(b,d)** External activity.

$y_{L/D}$ stays between 0 and 0.8 through the maturation. Since this value is always below 1, the Gaussian part of the line profile is at all times greater than the Lorentzian part. Just like the FWHM, $y_{L/D}$ is high when the strawberries are green and has its lowest values at late white. Despite this it goes high already when the berries are pink. Another noticeable feature is that all graphs go low at their ends, which indicates that the diffusion decreases as the strawberries are turning dry in the laboratory. The results do not change as wildly as the FWHM does at the red phase, which shows that the diffusion changes with the velocity in the object. The changes at white are very small.

FWHM and $y_{L/D}$ during maturation are illustrated in figure 26 in a matrix that summarises parts of the analysis above.

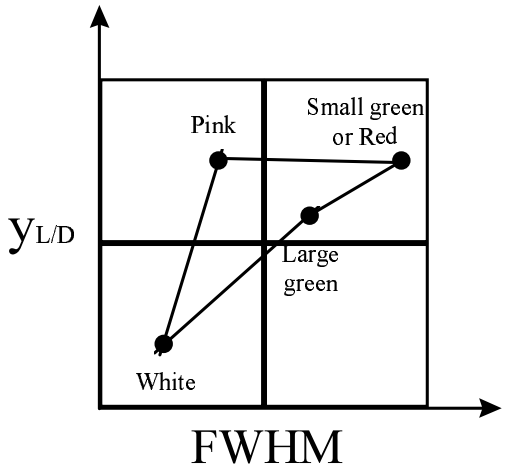

Figure 26. Summary of the changes in FWHM and $y_{L/D}$, due to the internal activity, as strawberries mature.

The two measures, FWHM and $y_{L/D}$, are compared in figure 27 to get an idea about the relation between them. Internally, the FWHM and $y_{L/D}$ follow each other through small changes but at the peaks they correspond to each other in opposite directions. This means that the small changes are due to diffusion which contributes positively to both measures. The peaks are mainly due to velocity changes which gives the inverse contribution to the $y_{L/D}$. Note that the highest peaks of $y_{L/D}$ appear when the strawberries are red. These velocity changes may be either a result from the breakage of the cells when the subparts start to flow among the other cells or from when the soft strawberries move sideways and thereby cause a moving speckle pattern. On the surface however, the FWHM and $y_{L/D}$ hardly follow each other at all. The only relation between these measures is that the (high) peaks in FWHM give opposite peaks in $y_{L/D}$. Besides this there are tendencies in the $y_{L/D}$ to go in opposite direction from the FWHM even at small changes. This tells us that the diffusion is not as important on the surface as it is inside the fruit.

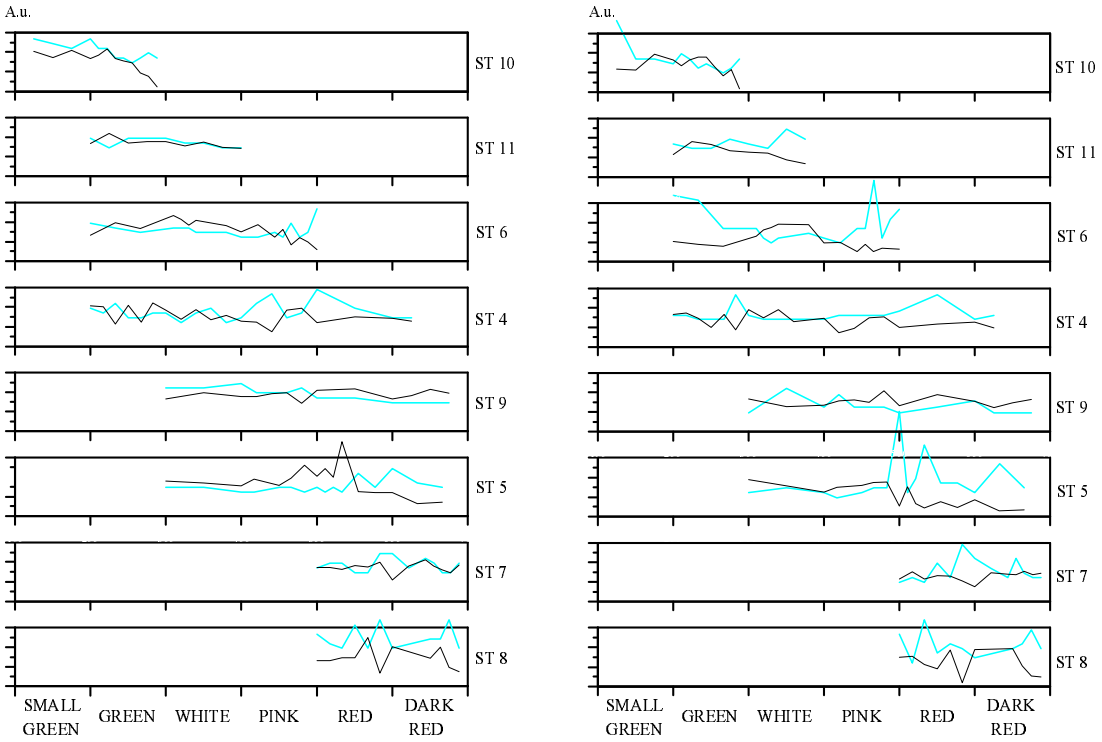

Figure 27. Comparison between FWHM (gray) and $y_{L/D}$ (black). Internal activity (left) and external activity (right).

4. Conclusion and discussion

The line profiles obtained from the Fourier transforms of the autocorrelations of the biospeckles' time histories show shifts due to Doppler effect, turbulence and diffusion in the objects. A Voight profile can describe it with FWHM and $y_{L/D}$ as the main features. With the FWHM it is possible to estimate the average velocity of the scatterers in the objects which turns out to be about $2\ \mu m/s$ in strawberries. The $y_{L/D}$ is the ratio of Lorentzian to Gaussian width and a measure of the diffusive movements in the object. If the laser beam is polarised it is possible to distinct the light scattered internally from the light scattered on the surface of the object. Nevertheless, the results are rather stochastic but have some interesting tendencies which the conclusions are based on.

Errors in the measurements are probably due to the changes in the environmental conditions, for instance temperature and atmospheric pressure, especially during the periods when the strawberries were measured twice a day. Furthermore, even though the temperature of the object do not increase much due to the laserbeam, it may still have an effect on the activity of the object and hence the results of the measurements. This is particularly important on the surface of the object since most light is absorbed there. The noise from the equipment comes mainly from the camera. It is measured to have the signal to noise ratio 1000, which is enough for what is necessary in this study. Most of the spectroscopical shifts of the light are too big for the detector and hence recorded as random noise. However, this type of noise is dismissed by the mean value of 512 autocorrelations and therefore, it does not interference with the measurements. The most important problem is probably Brillouin scattering due to vibrations and displacements transmitted from the building through the ground and the air. These vibrations might originate from building vibrations, people working in laboratories and ventilation ducts and are in the same range of frequencies as the shifts measured in this study. Some features of the noise were discovered in the experiments. The results from the activity on the surface is more stochastic than that from the internal activity. The noise has also greater effect on the Lorentzian part of the line profile than the Gaussian (equations 28 and 29), which can be seen in figure 27 where $y_{L/D}$ is more stochastic when measured externally than internally.

When different fruits were measured, it was discovered that the results vary with the different characteristics of the objects, but generally there is more activity inside the fruits and vegetables than on their surfaces. The results gave three groups of objects with similar characteristics, hard peel, thick peel or no peel. Thick peel gives high internal activity. The objects with neither thick nor hard peel show small differences between internal and external activity. For most of the vegetables the diffusion is greater on the surface than inside, though this is opposite for the fruits.

The characteristics of the Voight profile from the experiments with strawberries have different features depending on the maturity of the fruit. These results are summarised in figure 26. Figure 27 compares the two parameters FWHM and $y_{L/D}$, and shows that the activity on the surface mainly depends on the velocity of particles. It also indicates that it is possible to detect diffusion on the inside of the fruit, though it is difficult to

point out anything specific concerning the diffusion on the surface. When these tendencies are compared to the sugar flow, table 1, it is discovered that it has very little correlation with the diffusive movements in the strawberries. The flow is very slow when the strawberries are pink but, according to the measurements, this is the phase in the maturation where the diffusion reaches its highest values. When the diffusion was compared with physical changes in different stages of the maturation (see figure 20), only the flesh firmness was found to correlate with it. This suggests that the diffusion is a result from the movements of the cell walls which are more vivid as the firmness of the flesh decreases. It can be compared with a crystal of proteins which changes in elasticity. The FWHM correlates well with the amount of CO_2 but is probably a combination of the development of CO_2, the transportation of sugar and the changes in viscosity due to cellulose.

Future work in this field could improve and optimise the experiments and data processing in several areas. Primarily the results would probably be better if the environment of the strawberries were controlled and preferably constant. Furthermore, it would be interesting to study if the heating of the object due to the laser beam has an effect on the results. Also to increase the number of samples would probably improve the results. Further, to optimise the equipment with a faster camera and image processor makes it possible to detect more of the information that the present equipment dismisses as random noise. Presently it is possible to purchase a camera that takes 2000 pictures per second. Another possibility would be to use an array of detectors, which is faster than a camera. Though, the disadvantage would be that it can not detect 512 time histories simultaneously. The most important thing to do, however, is to get rid of the noise due to vibrations transferred through the building and the setup. One alternative would be to hang the setup in rubber straps from the ceiling. The technique eliminates the possibility for the setup to absorb frequencies lower than the resonance frequency of the setup, including the straps, which generally swings in a few hertz. This method is used in Scanning Tunnelling Microscopy (STM) and Atomic Force Microscopy (AFM) and can be further studied in [26,27]. To combine the experiments with spectroscopy would optimise the measurements even more, since the scattering radiates light with much more information than extracted in this study. The data processing can also be further optimised. In this work, the measures of the Voight profile is determined by two very characteristic positions on the line profile. Nevertheless, the profile contains more information that could be extracted if the whole line profile of the results were used. One example is to make a computer program that fits a Voight profile to the experimental results and gives the characteristics of it as an output. Another example is to separate the different types of broadenings from each other in the autocorrelation, equation 22. In this case, the Gaussian shape of the line profile is an e^{-x^2} function, and the Lorentzian an e^{-x} function.

If the work would be carried out with better equipment, more control of environmental factors and a greater amount of samples, it would probably be possible to construct an instrument to determine the maturity of fruits with the biospeckle technique.

Acknowledgements

First of all, I would like to express my most sincere thanks to my supervisor at Centro de Investigaciones Opticas (CIOp), Dr. Héctor J. Rabal, for all his support and engagement during my visit in Argentina, and my supervisor at LTH, Dr. Sven-Göran Pettersson. They made this thesis work possible and have been a great help throughout the work.

There are many other people at CIOp whose support and friendship I gratefully acknowledge. I would particularly like to thank Nelly Lucía Cap and Ricardo A. Arizaga, the two computer wizards of the Optics Group.

I would also like to thank Dr. Pedro Marcos Civello at the Centro de Investigaciónes y Desarrollo en Criotecnoligía de Alimentos (CIDCA) at Universidad Nacional de La Plata (UNLP) for his expertise help in issues concerning strawberries.

Special thanks are due to Joanna Lindbergh and Kristina Steeg for correcting the English in parts of the thesis.

The help and assistance from the Department personnel in Lund is also gratefully acknowledged.

Finally, I would like to express my appreciation to Lia Zerbino and her family for making me become a part of their family during my stay in La Plata.

5. References

[1] Rabal H J, Arizaga R A, Cap N L, Trivi M, Romero G, Alanís E. (1995)
”Transient phenomena analysis using dynamic speckle patterns, ”
Optical engineering vol. 35, no. 1, pp. 57-62.

[2] Ruth B. (1990)
”Blood flow determination by the laser speckle method, ”
Int J Microcirc: Clin Exp **9**: 21-45.

[3] Zheng B, Pleass C M, Ih C S. (1994)
”Feature information extraction from dynamic biospeckle, ”
Applied optics vol. 33, no. 2, pp. 231-237.

[4] Xu Z, Joenathan C, Khorana B M. (1995)
”Temporal and spatial properties of the timevarying speckles of botanical specimens,” Optical engineering vol. 34, no. 5, pp. 1487-1502.

[5] Vogelmann T C. (1993)
”Plant tissue optics,”
Annu. rev. plant physiol. plant mol. biol. vol. 44, pp. 231-251.

[6] Gausman H W, Allen W A, Escobar D E. (1974)
”Refractive index of plant cell walls,”
Applied optics vol. 13, no.1, pp. 109-111.

[7] Tuchin V V. (1993)
“Lasers and Fiber Optics in Biomedicine,“
Laser Physics vol. 3, no. 4, pp. 767-820.

[8] Svanberg S. (1992)
Atomic and molecular spectroscopy, Springer-Verlag.

[9] Bass M. (1995)
Handbook of optics I, 2nd ed., McGraw-Hill Inc.

[10] Lehninger A L. (1981)
Bioquímica, Las bases moleculares de la estructura y functión celular, 2nd ed.
Worth publishers, inc.

[11] Seyfried M, Fukshansky L. (1983)
”Light gradients in plant tissue,”
Applied optics vol. 22, no. 9, pp. 1402-1408.

[12] Bone R A, Lee D W, Norman J M. (1985)
”Epidermal cells functioning as lenses in leaves of tropical rain-forest shade plants,” Applied optics vol. 24, no. 10, pp. 1408-1412.

[13] Berg R. (1995)
Laser-based cancer diagnostics - Tissue optics considerations,
Lund reports on atomic physics, LRAP-184.

[14] Dainty J C, ed. (1975)
Laser Speckle and Related Phenomena, Springer-Verlag, Berlin.

[15] Goodman J W, (1984)
”Statistical properties of laser speckle patterns,”
Laser speckle and related phenomena, Dainty J C, ed., vol 9 of Topics in
Applied physics, Springer-Verlag, Berlin, pp. 9-75

[16] Drain L E, (1980)
The laser doppler technique chap. 4, p. 70, Wiley, New York.

[17] Briers J D. (1975)
”Wavelength dependence of intensity fluctuations in laser speckle patterns from biological specimens,” Opt. commun. vol. 13, pp. 324-326.

[18] Briers J D. (1993)
”Speckle fluctuations and biomedical optics: implications and applications, ”
Optical engineering vol. 32, no. 2, pp. 277-283.

[19] Goodman J W (1984)
Statistical optics.

[20] Gaskill J D. (1978)
Linear systems, fourier transforms and optics, p. 193,
John Wiley & sons, Inc.

[21] Asakura T, Takai N. (1981)
”Dynamic laser speckles and their application to velocity measurements of the diffuse object,” Applied optics vol. 25, no. 3, pp. 179-194.

[22] Friden B R. (1983)
Probability, statistical optics, and data testing,
Springer-Verlag, Berlin Heidelberg New York.

[23] Cummins H Z, Swinney H L. (1970)
Light beating spectroscopy,
chap. 3 in Progress in optics vol. VIII, pp. 133-200,, ed. Wolf E

[24] Thorne A P (1988)
Spectrophysics, 2nd ed., Chapman & Hall.

[25] Armstrong B H. (1967)
”Spectrum line profiles: the voight profile”,
J. Quant. Spectrosc. Radiat. Transfer. vol. 7, pp. 61-88, Pergamon Press Ltd.

[26] Bai C. (1995)
Scanning Tunneling Microscopy and its Application,
Springer-Verlag, Berlin Heidelberg.

[27] Wiesendanger R. (1994)
Scanning Probe Microscopy and Spectrosco py, methods and applications,
Cambridge University Press.

[28] Huber D J. (1984)
”Strawberry fruit softening: The potential roles of polyuronides and hemicelluloses,” Journal of food science vol. 49, pp. 1310-1315.

[29] Barnes M F, Patchett B J. (1976)
”Cell wall degrading enzymes and the softening of senescent strawberry fruit, ”
Journal of food science vol. 41, pp. 1392-1395.

[30] Manning K. (1993)
Soft fruit, chap. 12 in Biochemistry of fruit ripening,
ed. Seymour G, Taylor J, Tucker G, Chapman & Hall, London.

[31] John O-A, Yamaki S. (1994)
”Sugar content, compartmentation, and efflux in strawberry tissue, ”
J. Amer. Soc. Hort. Sci. vol. 119, no. 5, pp. 1024-1028.

Appendix

```
/*        FRUTY.C       */

/*          12-96          */

/*        For n number of objects, this program removes the head from a 512x512 image
file, subtracts the mean value of the time history of each pixel, autocorrelates the 512
time histories and takes the mean autocorrelation of them all as well as Fourier
transforms the autocorrelation. The following data is obtained for every image:
- files of autocorrelation,
- Fourier transform,
- re-scaled x-values for the power spectra to normalise it to be comparable with the
Voight
 profile,
- FWHM,
- y_{L/D} (importance of Lorentzian shape in the profile compared to the amount of
Doppler),
- mean value of the time histories and
- < I^2(0) > .     */

 /*       This program has the following inputs:
For each time the program is run:
- name of file containing inputs for every object to process,
- name of file for output of mean value of the time histories and
- name of file for output of  < I^2(0) > .
For every object:
- name of file containing number and names of images to process,
- name of file containing names of output files of autocorrelation,
- name of file containing names of output files of Fourier transform,
- name of file for output of FWHM and
- name of file for output of  y_{L/D} .       */

/*        The images must be in itex or vfg.     */

/*        Use FRUTYT.C to check that all the images are OK, so that you will not have a
break in the running of the program   */


#include "math.h"
#include "stdio.h"
#include "fft1opt.h"

main()
{
long auto1,auto2,g1,g2;
float a,v[56],w,vv,nor,g,sum,fwhm,partlor,lorentz,mod,
```

```
norr,min,meall,hmax,powsum,power,exx,xtot,mre=0,rer=0,rei=0;
int lm,p,x,r,j,k,l,q,acom,acome,comp,le[20],length,me,
o,m,halfn,z,isign,nn,n,size,size2,xdel,xval,tvax;
static int gris[1026],med[513],vect[513];
static float autoc[513],prom[1025],data[2050];
char nombre1[16],nombre2[16],nombre3[16],nombre4[16],nombre5[16],
nombre6[16],nombre7[16],nombre8[16],ca,lw,salida[15],nombre9[16],meansa[16];
FILE *arch1,*arch2,*arch3,*arch4,*arch5,*arch6,*arch7,*arch8,
*arch9,*meansal,*datsal;

printf("NAME OF FILE FOR OUTPUT OF MEAN VALUES? :\n");
scanf("%s",meansa);
meansal=fopen(meansa,"w");
printf("NAME OF FILE FOR OUTPUT OF < I^2(0) > ? :\n");
scanf("%s",nombre9);
arch9=fopen(nombre9,"w");
printf("NAME OF FILE CONTAINING INPUTS FOR EVERY OBJECT TO
PROCESS? :\n");
scanf("%s",nombre8);
arch8=fopen(nombre8,"rb");
fscanf(arch8,"%d",&size2);
for (r=1;r<=size2;r++){
fscanf(arch8,"%s",nombre3);
fscanf(arch8,"%s",nombre4);
fscanf(arch8,"%s",nombre7);
fscanf(arch8,"%s",nombre5);
fscanf(arch8,"%s",nombre6);
printf("STARTING FILE %s\n",nombre3);
arch3=fopen(nombre3,"rb");
arch4=fopen(nombre4,"rb");
arch5=fopen(nombre5,"w");
arch6=fopen(nombre6,"w");
arch7=fopen(nombre7,"rb");
fscanf(arch3,"%d",&size);
for (q=1;q<=size;q++){
        fscanf(arch3,"%s",nombre1);
        fscanf(arch4,"%s",nombre2);
        fscanf(arch7,"%s",salida);
        printf("AUTOCORRELATING IMAGE %s\n",nombre1);
        me=3;
        halfn=(me+1)/2;
        length=512-me+1;
        arch1=fopen(nombre1,"rb");
        arch2=fopen(nombre2,"w");
        datsal=fopen(salida,"w");
        for (x=1;x<=1024;x++){
                gris[x]=0;
                }
```

```
for (x=1;x<=512;x++){
        prom[x]=0.;
        }
/*      REMOVE THE HEAD OF THE IMAGE FILE       */
for(j=0;j<=13;j++){
        fscanf(arch1,"%c",&lw);
        le[j]=lw;
        }
acom=le[2]+10*le[3];
acome=acom+63;
/*      CHECK IF FILE IS COMPRESSED*/
comp=10*le[13]+le[12];
if(comp==1){
        printf("COMPRESSED!\n PRESS ANY KEY TO END");
        while(!kbhit());
        while(kbhit()==0);
        getch();
        goto xxx;
        }
if(comp==0){
        printf("NORMAL\n");
        }
for(k=14;k<=acome;k++){
        fscanf(arch1,"%c",&lw);
        }
norr=0;
meall=0;
/*      MAIN LOOP  */
for (p=0;p<512;p++){
/*      INSERT A FILE IN GRIS     */
        mean=0;
        for (j=1;j<=512;j++){
                fscanf(arch1,"%c",&ca);
                lm=ca;
                if(lm<0){
                        lm=lm+256;
                        }
                gris[j]=lm;
                mean=mean+lm;
                }
        min=mean/512;
        meall=meall+(min/512);
        /*      FILTER THE VECTOR FROM EXTREME PEAKS        */
        for (j=1;j<=512;j++){
                gris[j]=gris[j]-min;
                }
        if (me>1){
                for (k=1;k<=length;k++){
```

```
                for (m=1;m<=me;m++){
                        vect[m]=gris[k-1+m];
                        }
                for (o=1;o<me;o++){
                        for (j=o;j<=me;j++){
                                if (vect[o]>vect[j]){
                                        z=vect[o];
                                        vect[o]=vect[j];
                                        vect[j]=z;
                                        }
                                }
                        }
                med[k]=vect[halfn];
                }
        for (k=1;k<=me;k++){
                med[length+k]=0;
                }
        }
else{
        for (k=1;k<=512;k++){
                med[k]=gris[k];
                }
        }
for (j=1;j<=512;j++){
        gris[j]=med[j];
        }
/*      CALCULATE THE NORMALIZED AUTOCORRELATION
OF GRIS       */
auto2=0;
for (j=1;j<=length;j++){
        g1=(long)gris[j];
        auto2=(long)(auto2+g1*g1);
        }
nor=(float)auto2;
norr=norr+(nor/512);
for (j=1;j<=512;j++){
        autoc[j]=0.;
        }
for (x=0;x<512;x++){
        auto1=0;
        for (j=1;j<=length;j++){
                g1=(long)gris[j];
                g2=(long)gris[j+x];
                auto1=(long)(auto1+g1*g2);
                }
        autoc[x+1]=(float)(auto1/nor);
        prom[x+1]=(float)(prom[x+1]+autoc[x+1]);
        }
```

```
        }
/*      END OF MAIN LOOP        */
/*      DIVIDE PROM BY 512 AND PRINT IN FILE    */
for (x=1;x<=1024;x++){
        prom[x]=(float)(prom[x]/512.);
        if (prom[x]<=0){
                prom[x]=0;
                prom[x+1]=0;
                }
        j=2*x-1;
        data[j]=prom[x];
        data[j+1]=0;
        vv=prom[x];
        fprintf(arch2,"%f\n",vv);
        }
/*      FOURIERTRANSFORM THE AUTOCORRELATION IN DATA
*/
mre=0;
rer=0;
rei=0;
isign=1;
nn=1024;
n=2048;
/*      CALL THE SUBROUTINE FFT1OPT     */
fft1opt(data,nn,isign);
for(j=1;j<=n;j+=2) {
        rer+=data[j];
        rei+=data[j+1];
        mre+=data[j]*data[j]+data[j+1]*data[j+1];
        prom[(j+1)/2]=data[j];
        }
        /*      NOW WE HAVE A VECTOR PROM WITH THE
        POWERSPECTRA    */
        /*      CALCULATE THE FWHM  */
        fwhm=0;
        xdel=0;
        powsum=0;
        hmax=0.5*prom[1];
        for (x=1;x<=128;x++){
                if (prom[x]<hmax){
                        if (fwhm==0){
                                xdel=(hmax-prom[x])/(prom[x-1]-prom[x]);
                                xtot=x-1-((hmax-prom[x])/(prom[x-1]-prom[x]));
                                xval=x-1;
                                fwhm=2*xtot/(0.0802*1024);
                                fprintf(arch6,"%f\n",fwhm);
                                }
                        }
```

```
                }

        /*      NORMALIZE THE POWER SPECTRA TO THE TOTAL
        INTENSITY OF 50    */
        exx=1.66511/(2*xtot);
        for (x=1;x<=512;x++){
                powsum=powsum+exx*prom[x];
                }
        for (x=1;x<=512;x++){
                vv=(50/powsum)*prom[x];
                exx=1.66511*x/(2*xtot);
                fprintf(datsal,"%f\t%f\t%f\n",exx,prom[x],vv);
                }
        /*      CALCULATE THE LORENTZ/GAUSS VALUE   */
        if (xdel>0.5){
                tvax=2*xval;
                lm=prom[tvax]+(2*xdel-1)*(prom[tvax]-prom[tvax-1]);
                }
        else{
                tvax=2*xval+1;
                lm=prom[tvax]+(2*xdel)*(prom[tvax]-prom[tvax-1]);
                }
        lorentz=prom[1]/lm;
        power=pow(lorentz,exp);
        partlor=3.43315/power;
        fprintf(arch5,"%f\n",partlor);
        fprintf(arch9,"%f\n",norr);
        fprintf(meansal,"%f\n",meall);
        fclose(arch1);
        fclose(datsal);
        fclose(arch2);
        }
    fclose(arch3);
    fclose(arch4);
    fclose(arch5);
    fclose(arch6);
    fclose(arch7);
    xxx:;
    }
fclose(arch9);
fclose(arch8);
fclose(meansal);
}
```